

**Magnetic susceptibility in the European Loess Belt: new and existing models of
magnetic enhancement in loess**

Balázs Bradák^{1,*}, Yusuke Seto², Thomas Stevens³, Gábor Újvári^{4,5}, Katalin Fehér⁶,
Chiara Költringer³

¹Department of Physics, University of Burgos, Av. de Cantabria, s/n 09006, Burgos,
Spain

²Department of Planetology, Kobe University, Nada, Kobe, 657-8501, Japan

³Department of Earth Sciences, Uppsala University, Villavägen 16, Uppsala, 75236,
Sweden

⁴Department of Lithospheric Research, Univ. of Vienna, 14 Althanstrasse, Vienna,
Austria, A-1090

⁵Institute for Geological and Geochemical Research, Research Centre for Astronomy and
Earth Sciences, 45 Budaörsi St., Budapest, Hungary, H-1112.

⁶ ELTE Eötvös Loránd University, Institute of Geography and Earth Sciences,
Department of Environmental and Landscape Geography, Pázmány Péter sétány 1/C.
Budapest, Hungary, H-1117

19

20 *Corresponding author: Balázs Bradák, bradak.b@gmail.com

21 Yusuke Seto: seto@crystal.kobe-u.ac.jp; Thomas Stevens: thomas.stevens@geo.uu.se;

22 Gábor Újvári: Ujvari.Gabor@csfk.mta.hu; Katalin Fehér: feher.katoke@gmail.com;

23 Chiara Költringer: chiara.koltringer@geo.uu.se

24

25

26 Abstract

27 Magnetic susceptibility measurements play a key role in Quaternary studies.

28 Magnetic proxies, such as low field and frequency-dependent magnetic susceptibility, are

29 widely applied in the reconstruction of terrestrial paleoclimate, e.g., in the study of loess-

30 paleosol successions. In general, the interpretation of loess magnetic susceptibility signals

31 is based on two commonly accepted models: the pedogenic magnetic enhancement and

32 wind-vigour models. However, there are an increasing number of cases where such

33 models cannot be used. These cases show unusual relationships between the two common

34 loess magnetic susceptibility proxies: low field and frequency-dependent magnetic

35 susceptibility. Such relationships have been attributed to various phenomena including

36 the dissolution of fine-grain minerals and the formation of ultrafine magnetic rims on the

surface of coarser grains by weathering. Despite the growing number of these exceptional cases of magnetic enhancement, our knowledge about the occurrence and potential causes of the unusual behaviour of magnetic susceptibility parameters is still limited. This, in turn, hinders the wider application of magnetic susceptibility parameters in loess. To fill this knowledge gap, magnetic susceptibility data of various profiles from the European Loess Belt were collected and compared to reveal various enhancement trends in loess. Along with the analysis of magnetic susceptibility parameters, combined scanning electron microscopy (SEM) and rock magnetic analyses were applied to samples from the Paks loess sequence in Hungary to describe some of the irregular cases, notably the cause of increasing frequency-dependent susceptibility in non-altered sediments. Analysis of loess, paleosol and common mineral samples separated from loess (e.g., muscovite) revealed that various features may be responsible for these increasing frequency-dependent susceptibility values: i) surface weathering (maghemitization) of coarser detrital grains, ii) nanofragmentation by physical weathering and iii) the appearance of significant amounts of ultrafine magnetic inclusions in micas. These special modes of magnetic enhancement of loess do not undermine the importance of the basic theories suggested above, but rather provide three mechanisms that account for some of the increasing number of unusual cases. To aid in the wider and more accurate use of

magnetic susceptibility parameters in loess, we review the current magnetic enhancement models with special emphasis on the identification of unusual trends in magnetic enhancement and understanding their drivers.

Keywords: magnetic susceptibility; loess; magnetic enhancement; nano-scale fragmentation; magnetic inclusion

Abbreviations: CLP-Chinese Loess Plateau; EDS-energy-dispersive X-ray spectroscopy; ELB-European Loess Belt; EXT-extract by strong magnet; χ_{lf} -low field magnetic susceptibility; χ_{fd} -frequency dependent magnetic susceptibility; χ_{fs} -normalized frequency dependent magnetic susceptibility; MIS-marine isotope stage; MD-multidomain; PSD-pseudo-single domain; RESIDc-coarser grained (>125 μm) residual after extraction by strong magnet; RESIDf-finer grained (<125 μm) residual after extraction by strong magnet; SD-single domain; SEM-scanning electron microscope; SP-superparamagnetic; Tc-Curie temperature; VS-vortex state;

1. Introduction

The nature of glacial and interglacial paleoenvironments and their role in understanding future climates has become a major focus of Quaternary research over recent decades (PAGES, 2016). As a part of the reconstruction of paleoenvironment, increasingly more information has been revealed about loess records, which are some of the most commonly used terrestrial archives in the reconstruction of glacial and interglacial paleoenvironment over the Quaternary (Pye, 1987). In such reconstructions, mineral magnetic methods play a crucial role since both the type and amount of magnetic contributors in loess are highly sensitive to environmental change during pedogenesis (Maher and Taylor, 1988; Heller et al., 1993; Forster et al., 1994; Dearing et al., 1996; Maher, 2011, 2016). In fact, basic frequency-dependent magnetic susceptibility analysis has become a routine stratigraphic tool in studies of loess sequences (e.g., Schatzel et al. 2018 and references therein).

There are two commonly known models for the enhancement of the magnetic susceptibility parameters in loess: pedogenesis and wind vigour (e.g., Forster et al., 1994; Evans and Heller, 1994; Evans, 2001). Both models were built to describe the rhythmic change of environmental magnetic proxies, especially magnetic susceptibility parameters, in loess sequences, most likely related to the cycles of glacial (stadial) and interglacial

(interstadial) periods. The widely accepted main magnetic enhancement models seem highly variable geographically. Additionally, there is no consensus about the applicability of the alternative models, and apparently, a number of different hypotheses appear in the literature (see Section 2). Due to the common use of χ_{lf} and χ_{fd} , it is essential to resolve these inconsistencies and ambiguities so that these widely used proxies can properly inform debates about past environmental changes. This requires understanding of the fundamental physical meaning of magnetic parameters. The primary goal of this study is to reveal potential influences on magnetic mineral components in sediments that exhibit unusual χ_{lf} and χ_{fd} using examples from the Paks loess section in Hungary.

2. The overview of magnetic enhancement models in loess characterized by the relationship between χ_{lf} and χ_{fd} parameters

2.1 Pedogenic enhancement model and the “true loess line”

The pedogenic model explains the magnetic enhancement of loess by in situ authigenic mineral formation (Maher and Taylor, 1988; Heller et al., 1993; Forster et al., 1994; Dearing et al., 1996; Maher, 2011, 2016). This leads to increased low field magnetic

susceptibilities (χ_{lf}) and frequency-dependent magnetic susceptibilities (χ_{fd}) in soils formed over interglacials, offering favourable conditions for the formation of ultrafine superparamagnetic (SP) components, such as warmer temperatures and more humid environments (higher precipitation). This relationship between precipitation and mineral neoformation allows for quantitative paleoprecipitation estimation using mineral magnetic methods (e.g., Heller et al., 1993; Maher et al., 1994, 2002, 2003; Panaiotu et al., 2001; Geiss and Zanner, 2007; Geiss et al., 2008; Balsam et al., 2011; Orgeira et al., 2011; Long et al., 2016).

One of the commonly applied mineral magnetic methods used in paleoprecipitation estimation is the measurement of χ_{fd} . χ_{fd} analysis has been applied since the pioneering studies of Forster et al. (1994) and Dearing et al. (1996) as a sensitive indicator of ultrafine magnetic grains, increasing amounts of which also influence χ_{lf} . This linear relationship between increasing χ_{fd} and χ_{lf} was recognized in many loess successions of the European Loess Belt (ELB) and the Chinese Loess Plateau (CLP) and is called the pedogenic enhancement model (Zhou et al., 1990; Forster et al., 1994; Evans and Heller, 1994; Evans, 2001). The relationship between the two susceptibility parameters, i.e., the trend described by χ_{lf} and χ_{fd} , has been used since publication of the above studies to recognize pedogenic enhancement in loess sequences (e.g., Maher, 2011; Maher, 2016, and the

references therein). Following the study of Maher (2016), where the magnetic enhancement models were summarized, Zeeden et al. (2016, 2018) defined the so-called true loess line. The “true loess line” is a linear trend fitted to χ_{lf} and χ_{fd} data, describing the magnetic enhancement trend of loess during pedogenesis driven by increasing neoformation of magnetic minerals. Although the term “true loess line” was first introduced in Zeeden et al. (2016), variations of the χ_{lf} vs. χ_{fd} plot and the “true loess” trend have been commonly used since the loess studies of the 1990s (e.g., Forster et al., 1994; Panaiotu et al., 2001; Maher, 2011).

2.2 Deviation from “true loess line” and other enhancement models

As summarized by Maher (2011) and Zeeden et al. (2018), deviation from the “true loess line” may indicate additional processes that, along with pedogenesis, contribute to the magnetic enhancement of loess. The deviations appear in various ways in the χ_{lf} vs. χ_{fd} plot. Compared with pedogenic enhancement, some loess sequences are characterized by relatively high χ_{lf} compared with the soil horizons (e.g., Begét and Hawkins, 1989). In other cases, some well-developed soil horizons may not show high χ_{fd} values (e.g., Taylor et al., 2014). There are sediments surprisingly characterized by low χ_{lf} but relatively high χ_{fd} (Wacha et al., 2018). In this sense, the “true loess line” does not seem to be always

applicable to loess records, as there are loess deposits in the broader sense of wind-blown terrestrial silt deposits showing deviations from this line. Such discrepancies and their possible causes are described in detail below.

2.2.1 Wind-vigour model

In contrast to the pedogenic model, the wind-vigour model explains observations of higher χ_{lf} values in loess (rather than palaeosols) as a result of the enrichment of coarser grained magnetic minerals in the units of coarse grained loess (Evans, 2001). Increasing magnetic susceptibility during glacial periods was originally described by Begét and Hawkins (1989) from Alaskan loess. Following this study, magnetic enhancement due to wind vigour has been reported from various loess regions (Chlachula et al., 1998; Wang et al., 2006; Kravchinsky et al., 2008). Notably, Chlachula et al. (1998) found the characteristics of wind-vigour enhancement in Siberian loess. Wind-vigour enhancement is rare in the European Loess Belt, except for the cases reported in Zeeden et al. (2018) and Wacha et al. (2018). In both cases, the wind-vigour model is not the only process responsible for the magnetic enhancement but rather works in line with pedogenic processes.

Based on an analysis of Pampean loess, Bidegain et al. (2005) suggested the appearance of both pedogenic and wind-vigour magnetic enhancement in the same loess

record. This phenomenon was further confirmed in Siberian loess, where Kravchinsky et al. (2008) found that while loess units display higher χ_{lf} than paleosol horizons, paleosols exhibit higher χ_{fd} , indicating mineral neoformation, such as ultrafine pedogenic magnetite/maghemite grains. A similar pattern was also reported by Wang et al. (2006) in the NE Tibetan Plateau and by Liu et al. (2012) in east Central Asia (Talede loess, Yili basin, Tianshan Mountains).

The recent study from Pegwell Bay loess (Stevens et al., 2020), also shows more complex control on the enhancement of magnetic susceptibility. Although significant increase of frequency dependent magnetic susceptibility was recognized by the increase of χ_{lf} , a significant discrepancy can be observed between the trend of Pegwell Bay and the “true loess line”. Along with the pedogenic enhancement, the allocation of the data and its trend suggested the appearance of wind vigour enhancement in the “lower calcareous loess unit” (Stevens et al., 2020; p. 13).

2.2.2 Dissolution, magnetic depletion, and grain surface weathering

Along with the wind-vigour effect, relatively high χ_{lf} and low χ_{fd} compared to typical loess, represented by the “true loess line”, may indicate the dissolution of magnetic contributors by hydromorphic effects (Taylor et al., 2014). Particle dissolution due to

waterlogging may affect ultrafine-grain single domain (SD) and small pseudosingle domain (PSD) particles before dissolving coarser multidomain (MD) magnetic particles. The dissolution of fine magnetic grains leads to a decrease in the concentration of ultrafine-grain components (e.g., the SP contributors responsible for χ_{fd}) and an increase in the mean magnetic grain size of the sediment (Taylor et al., 2014).

The effects of magnetic depletion also appear in the model of Zeeden et al. (2018), where the relatively low χ_{lf} but high χ_{fd} and $\chi_{fd}\%$ are driven by hydromorphic processes and/or intense weathering, as suggested by Baumgart et al. (2013). However, increasing ultrafine magnetic contributions cannot be described by hydromorphic processes, which, based on the theory of Taylor et al. (2014), would dissolve the finer components first and result in decreasing χ_{fd} .

Both wind-vigour and mineral dissolution effects result in relatively high χ_{lf} but low χ_{fd} . This begs the question of why some loess/paleosol layers in the ELB exhibit low χ_{lf} but high χ_{fd} (or $\chi_{fd}\%$) (Baumgart et al., 2013; Buggle et al., 2014; Maher, 2016; Zeeden et al., 2016, 2018). These phenomena appear in parts of loess profiles where the pedogenic enhancement model can otherwise be applied: generally, loess yields comparatively lower χ_{lf} and χ_{fd} ($\chi_{fd}\%$: <5%), while the soil horizons have higher χ_{lf} and χ_{fd} (~10% or above) (e.g., Dearing et al., 1996). The appearance of enhancement trends different from the “true

loess line” suggests that in addition to pedogenic enhancement, additional processes are operating.

Baumgart et al. (2013), supported by the model of van Velzen and Dekkers (1999), suggest that decreasing magnetic grain sizes caused by strong chemical weathering of larger primary particles is the cause of increasing χ_{fd} concurrent with relatively low χ_{lf} in paleosols. Chemical alteration as a possible cause of low χ_{lf} compared to relatively high χ_{fd} in Australian loess was also suggested by Ma et al. (2013).

One theory stems from observations by Wacha et al. (2018) of “detrital magnetic enhancement” in sediments from Susak (Croatia). In the study area, the trend of magnetic parameters of sandy loess displayed similar tendencies to paleosols (increasing χ_{lf} and χ_{fd}). Based on the magnetic experiments and observations of Buggle et al. (2014), Wacha et al. (2018) explained the “detrital magnetic enhancement” as a result of surface oxidation of the MD magnetic fraction and therefore formation of ultrafine SP grains on the surface of coarser detrital grains. A similar theory appeared in Zeeden et al. (2018), which suggests oxidation in source areas before the transportation of dust to form loess. The oxidation of unweathered particles may create an oxidized rim consisting of ultrafine magnetic minerals around an unaffected core, resulting in higher χ_{lf} and χ_{fd} compared to unweathered particles (Buggle et al., 2014; Wacha et al., 2018).

The data from the “upper non-calcareous unit” of Pegwell-bay loess (a profile with complex pattern of magnetic susceptibility enhancement) shows a shallower line of increased magnetic susceptibility parameter values compared to the “true loess line”. This trend “may suggest some pedogenic enhancement but may also indicate hydromorphic alteration of magnetic minerals under redox conditions, leading to dissolution of magnetic particles (Stevens et al. 2020; p. 13).

2.3 Beyond the relationship between common magnetic susceptibility parameters

Although the focus of this study is the relationship between two commonly used magnetic susceptibility parameters, χ_{lf} and χ_{fd} , and their significance in the reconstructions of environmental processes, there are a great number of studies that concentrate on the magnetic mineral alteration and neoformation in loess paleosol sequences more widely, particularly focussing on goethite, magnetite, maghemite and hematite (e.g. Boyle et al., 2010; Jiang et al., 2018, and the references therein). Such studies apply combined rock magnetic and geochemical (mostly diffuse reflectance spectroscopy – DRS) methods and have played a significant role in the understanding of magnetic enhancement of loess during pedogenesis, as summarised briefly below.

The early studies of combined magnetic and DRS research by Ji et al. (2001, 2002,

2004) contain the essential elements of this research line: redness (and other) colorimetric indices, the hematite/goethite ratio and the joint application of DRS and other climatic proxies. Following these first steps, Torrent et al. (2007) applied a combined rock magnetic and DRS method to describe the origin of various iron oxides, especially magnetite, maghemite and hematite and oxyhydroxide (goethite) in paleosols from the CLP. The proposed model concerning the pathway by which ferrihydrite is transformed into a transient maghemite-like phase before its final transformation into hematite was verified by the study of Hu et al. (2013). The study of Liu et al. (2011) verified the reliability of the DRS method in the quantification of the amount of hematite present and provided additional information about the potential bias in the method. Jiang et al. (2013) applied magnetic and DRS experiments and provided evidence concerning the aeolian origin of goethite in Chinese loess. The recent study of Jiang et al. (2018) provides a five-stage model about the magnetic mineral alteration (with a focus on magnetite, maghemite and hematite) in soil, which fundamentally changes the conventional model by providing detailed steps and description of mineral alteration and neoformation, proposed by e.g. Barrón and Torrent (2002), Barrón et al. (2003), and Liu et al. (2008).

Although a great amount of combined rock magnetic and DRS studies attempting to understand the chemical pathways of pedogenic enhancement have been elaborated in

Chinese loess, there is also some research on this on the ELB. Bábek et al. (2011) elaborated joint magnetic (e.g. magnetic susceptibility) and DRS study on Dolní Věstonice (Czech Republic) and Krasnogorskoye loess sections (SW Siberia, Russian Federation). The applied methods seemed to work well in the correlation of single successions, but the study also concluded that there is no universal proxy for weathering or pedogenesis intensity which can be applied across broad regions or along considerable climatic gradients (e.g., in continental scale). The observations of Bábek et al. (2011) raise some concern about the application of various magnetic and non-magnetic proxies and models in the case of various types of paleosols and continental scale correlations based on magnetic susceptibility. Paleosols, developed under paleomonsoon climate characterized by significantly higher precipitation might show different weathering characteristics and different degree of (magnetic) mineral alteration than the paleosols developed under Atlantic or continental climatic influence, for example. In addition, the varying magnetic mineral composition of the parent material of the soil (i.e. loess) may impact the magnetic mineral composition of soils (e.g., in some cases higher concentrations of hematite may appear in loess; Bradák et al. 2019a).

3. Materials and methods

3.1 Material

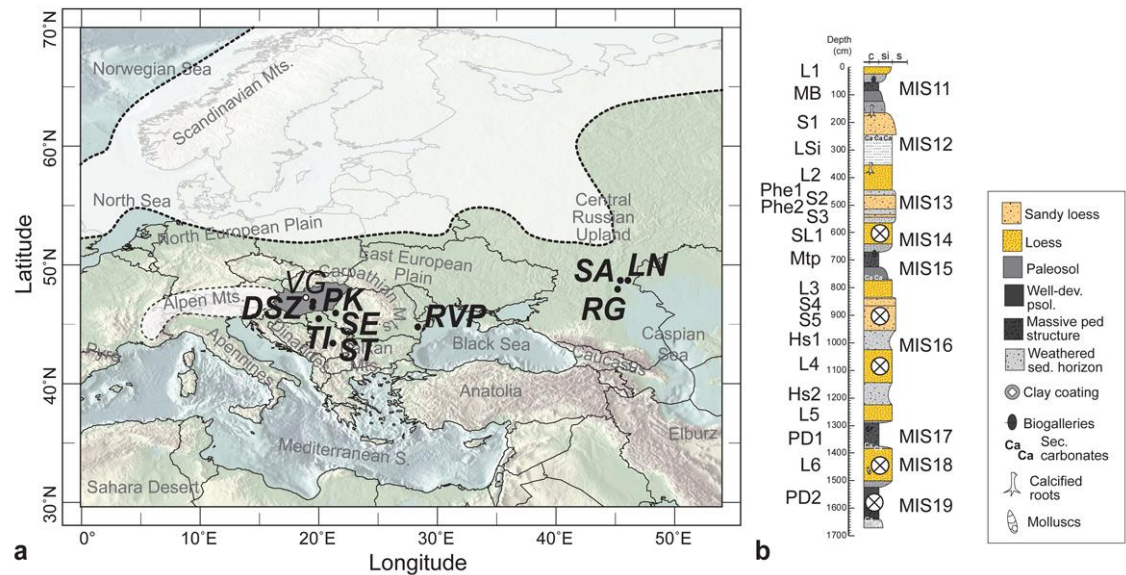


Figure 1. The geographical location of the Paks profile (Hungary) and other successions where magnetic parameters were analysed in this study (a) and the studied sequence with sampled units of the Paks loess-paleosol sequence (b). The abbreviations of the profiles are as follows: Dunaszekcső - DSZ, Leninsk - LN, Paks - PK, Raigorod - RG, Rasova-Valea cu Pietre – RVP, Srednaya Akhtubá – SA, Stalac section – ST, Semlac – SE and Titel – TI loess. The circles with crosses indicate the sampling points for rock magnetic and SEM measurements from the Paks profile. The abbreviations of stratigraphic units in the Paks record are as follows: L1-6 loess, SL1-sandy loess; S1-5 very fine sand, MB – Mende Base paleosol, Phe1, Phe2 - Paks sandy soil complex, Mtp

- hydromorphous soil at Paks, Hs1 and 2 – weathered sandy loess horizons, PD1 - Paks Double 1 paleosol, PD2 - Paks Double 2 paleosol. Detailed information about these units can be found in Bradák et al. (2019a and b) and in Supplementary Material 1. The boundary of glacial ice sheets in the study area was reconstructed using the works of Toucanne et al. (2009) and Batchelor et al. (2019). The basic relief map is from Amante and Eakins (2009).

The Paks loess profile is located to the north of the town of Paks in the Pannonian Basin, Hungary, on the right bank of the Danube River 46°38'24''N and 18°52'24''E, top of the sequence: ~135 m a.s.l.; Fig. 1a) (Újvári et al., 2014). The glacial deposits, corresponding to marine isotope stage (MIS) 18, MIS16, MIS14, MIS12 and MIS10, are represented by various aeolian sedimentary units (loess - L, sandy loess - SL, and fine sand - S) in the studied section at Paks (Suppl. Mat. 1a, b and c). Interglacial deposits (MIS19, MIS17, MIS15, MIS13 and MIS11) are represented by various paleosols intercalated with sediment units such as PD2, PD1, Hs1-2, Mtp, Phe2-1 and MB (Újvári et al., 2014; Marković et al., 2015) (Fig. 1b; Suppl. Mat. 1d, e, f and g). As part of a recent sampling session for a detailed magnetic study at Paks, a 16-m thick loess/palaeosol sequence was cleaned and sampled (Fig. 1b). Block samples were taken every 10 cm.

From each block, approximately 5 to 10 pieces of 2-cm³ cube samples were prepared for further analysis (sum. 950 samples) (Fig. 1b). Detailed information about the units of the sampled section can be found in Bradák et al. (2018a, b and 2019a, b and Suppl. Mat. 1). The mass of the samples was used to compare the magnetic enhancement characteristics of the studied section in Paks loess with various loess successions from the ELB (Fig. 1a). Magnetic susceptibility data were collected and used from Költringer et al. (2020), Marković et al. (2011), Obreht et al. (2016), Újvári et al. (2016), and Zeeden et al. (2016, 2018). The abbreviations of the datasets (profiles) used in the manuscript are the following: Dunaszekcső - DSZ, Leninsk - LN, Paks - PK, Raigorod - RG, Rasova-Valea cu Pietre – RVP, Srednaya Akhtuba – SA, Stalać section – ST, Semlac – SE and Titel – TI loess (Fig. 1). Due to the nature of the study, i.e., focusing on the magnetic enhancement trends and the comparison of the applicability of the “true loess line” in various successions, no detailed vertical characterization of the magnetic proxies from the Paks profile was executed. Such analysis can be found in Bradák et al. (2018a, b and 2019) and will be published in further studies in the near future.

Along with the samples used for susceptibility measurements, pilot samples were collected from various sediment layers of the Paks (PK) sequence, including the SL1, S5, L4 and L6 sediment units and PD2 paleosol horizon (Fig. 1b). These pilot samples

represent aeolian loess (L4 and L6) and paleosol (PD2) horizons and units with uncommon magnetic susceptibility parameters, such as low χ_{lf} but relatively high χ_{fd} (SL1 and S5).

The material of L6 went through further preparation to reveal additional information about the magnetic enhancement of sediments. The aggregates appearing in loess were disintegrated by an ultrasonic bath. The finest clay contributors were separated from the coarser grain (silt and sand) mixture by a laboratory centrifugal separator (MLW Centrifuge T 52.1; Labexchange, Germany). Following the removal of clay components, the material of L6 was separated into two components by a strong magnet, placed into a plastic tube and immersed in the suspension for 24 hours. After removing the magnet from the suspension, the strong magnetic components of L6, attached to the wall of the plastic tube, could be collected separately (Suppl. Mat. 2). This “extract” (EXT) mainly contains ferromagnetic minerals. The residual (RESID) was further separated into two groups by a sieve: a finer, mainly silt and fine sand grain size group ($<125\ \mu\text{m}$; RESIDf) and a coarser sand grain size group ($>125\ \mu\text{m}$; RESIDc). From the magnetic mineral point of view, RESID groups mainly contain dia- and paramagnetic components (e.g., phyllosilicates; Suppl. Mat. 2).

3.2 Methods

The low frequency (~0.5 and ~0.9 kHz) and high frequency (~4 and ~16 kHz) magnetic susceptibilities of ~2-cm³ Paks samples were measured in the laboratory using an SM 100 portable susceptibility meter (ZH-Instrument, Brno, Czech) (Suppl. Mat. 3 and 4). Please note that for the SM 100, the sensitivity is $\sim 5 \times 10^{-6}$ SI units at 0.5 kHz and 1×10^{-6} SI units for 4 and 16 kHz frequencies.

To determine χ_{fd} , the susceptibility of the samples was measured at low and high frequencies. Absolute (χ_{fd}) and relative frequency dependence of magnetic susceptibility ($\chi_{fd\%}$) were used in environmental magnetic studies. The former is defined by the following:

$$\chi_{fd} = \chi_{lf} - \chi_{hf} \quad (1)$$

which was used in this and numerous previous studies (e.g., Dearing et al., 1996; Zeeden et al., 2016 and the references therein). χ_{fd} is a strongly operating frequency-dependent parameter (e.g., Hällberg et al., 2020); therefore, Hrouda (2011) proposed the use of χ_{fd} normalized by the differences of the natural logarithm of the applied high and low frequencies:

$$\chi_{fs} = (\chi_{lf} - \chi_{hf}) / (\ln f_{hf} - \ln f_{lf}) \quad (2)$$

where χ_{fs} is the normalized χ_{fd} , and f_{lf} and f_{hf} are the low and high frequencies used during the experiments, respectively.

The use of χ_{fs} allows us to compare previously measured magnetic susceptibility data from various profiles obtained by different instruments. Since early studies in frequency-dependent magnetic susceptibility analysis of loess, there has been significant technical development in instrumentation, resulting in a wide range of applicable frequencies and sensitivities. As a result of such technical development, the widely used χ_{fd} and $\chi_{fd\%}$ parameters are biased by the various measuring frequencies that differ between instrument models. This bias or difference must be considered during the comparison of results from various profiles measured by various instruments. The normalization process suggested above provides a way to address such bias and makes data from various origins comparable. Following the calculation of χ_{fs} , a χ_{lf} and χ_{fs} plot can be used to characterize the relationship between the χ_{lf} and χ_{fs} of sediment and paleosol samples. The background susceptibilities were determined following the method of Panaiotu et al. (2011) by using the normalized frequency dependence of magnetic susceptibility. Background magnetic

susceptibility represents the magnetic susceptibility of sediments without any pedogenic enhancement, i.e., without the influence of neoforming pedogenic magnetic components (Table 1 and Suppl. Mat. 4).

To estimate the domain state of magnetic components, hysteresis measurements were conducted using a Micromag 2900 AGM with an alternating gradient field magnetometer (Princeton Measurements Co.) and variable field translation balance (VFTB, Mag Instruments UG, Germany) (Suppl. Mat. 3 and 4). A maximum applied field of 1 T (the limitation of both instruments) was used for the hysteresis measurements. During the hysteresis measurements the following settings were used for Micromag AGM: field range - 1, moment range - 50×10^{-9} , averaging time - 100×10^{-9} ; and for the VFTB: dwell time - 1s, gain -1, and data cycles and wait cycles – 15 and 10.

The coercivity of remanence (remanent coercive force) to coercivity ratio (H_{cr}/H_c) and saturation remanence to saturation magnetization (M_{rs}/M_s) plot, the so-called Day plot analyses (Day et al., 1977; Dunlop, 2002), were used to reveal the multidomain, single-domain (SD), superparamagnetic (SP) and pseudo-single domain (PSD) (in later studies: SD + MD mixture; Dunlop, 2002; or vortex state [VS]; Roberts et al., 2017) state of the magnetic mineral components in the samples (Suppl. Mat. 3 and 4).

Thermomagnetic experiments (temperature dependence of magnetization) were also

carried out by VFTB from room temperature (~20-25 °C) up to 700 °C in air. The following parameters were applied during the thermomagnetic experiments: dwell time - 1s, dwell field - 35mT, ramp slope - 30 °C/min, data cycles - 10, and wait cycles - 2. Temperature variation in magnetization provides information about the transformation, e.g., the Curie temperature (T_c) of magnetic mineral components identifies the change in magnetic moment at different temperatures during heating and cooling (Suppl. Mat. 3 and 4).

The results of rock magnetic measurements were analysed by RockMagAnalyzer1.1 software (Leonhardt, 2009). During the analysis of hysteresis curves, all parameters were corrected using their dia- and paramagnetic fractions.

Well-polished samples were studied by using a JSM-6480LAI scanning electron microscope (SEM; JEOL, Tokyo, Japan) equipped with energy-dispersive X-ray spectroscopy (EDS), and a JXA-8900 electron probe microanalyser (EPMA) with a wavelength-dispersive X-ray spectrometer. To obtain flat and smooth surfaces, we impregnated the samples with a low-viscosity resin (Petropoxy 154) and polished them using SiC and Al_2O_3 abrasives without lubricant to avoid alteration of clay minerals. For SEM observations, we used back-scattered electron imaging. Chemical analyses using EDS were obtained at 15 kV and 0.4 nA. Data corrections were made by the ZAF method

with well-established natural/synthesized materials as chemical standards.

4. Results

4.1 Magnetic enhancement trends from ELB

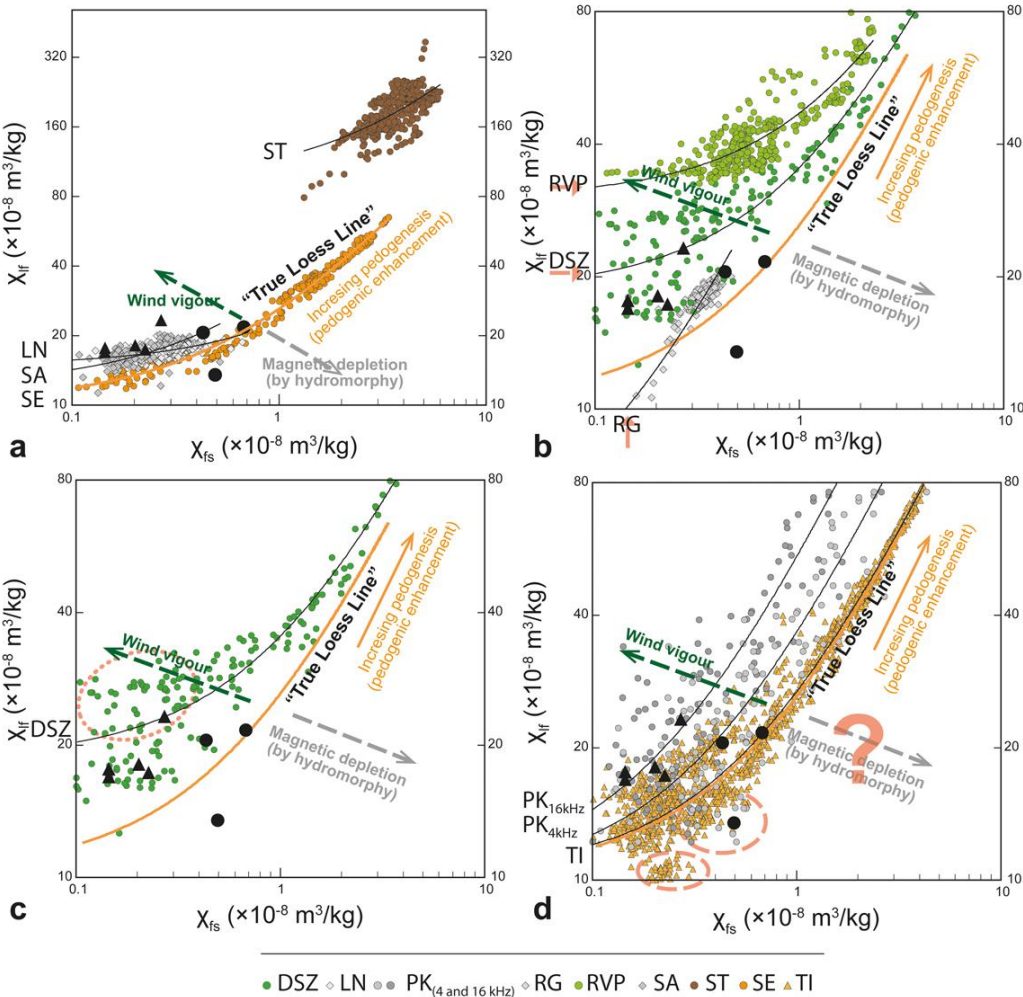


Figure 2. The complex magnetic enhancement model introduced by Maher (2011)

and Zeeden et al. (2018). a) Samples with weak mathematical statistical relationships

between the magnetic susceptibility parameters (LN, SA and ST) and the samples from the SE profile, characterized by the true loess line. b) Irregular background susceptibility (indicated by the red arrow for DSZ, RG and RVP). c) Discrepancy towards the “wind-vigour” region (red dotted circle) from the main magnetic enhancement trends (DSZ sequence). d) discrepancy towards the “magnetic depletion” region (red dotted circle) from the main magnetic enhancement trends (PK and TI sequences). The triangles and circles indicate pilot samples from the PK site where EXT, RESID_f and c contributors were separated (triangles; see 2.1) for further magnetic analysis. The black circles represent sediment samples with irregular H_{cr}/H_c and M_{rs}/M_s values on Figure 4. The sources of magnetic susceptibility data are Költringer et al. (2020), Marković et al. (2011), Obreht et al. (2016), Újvári et al. (2016) and Zeeden et al. (2016, 2018).

A set of χ_{lf} and χ_{fs} data from various profiles of the ELB were used to verify the existence of the “true loess line”, the trend of magnetic enhancement of aeolian sediments by pedogenic processes (Zeeden et al., 2018) (Fig. 2). Most of the data from profiles of various regions exhibit a positive correlation between χ_{lf} and χ_{fs} (average correlation coefficient, r_{AVG} : 0.89), which suggests the pedogenic enhancement of magnetic susceptibility by SP particles. Low correlation coefficients among the studied sections

were found at SA ($r = +0.56$, $p(a) < 0.05$, $n = 103$), LN ($r = +0.57$, $p(a) < 0.05$, $n = 315$) and ST ($r = +0.67$, $p(a) < 0.05$, $n = 410$) (Table 1; Fig. 2a). In some loess profiles, namely, RVP, DSZ and RG, the trend of magnetic enhancement was similar to the “true loess line” (increasing χ_{lf} and χ_{fs}), but significant deviations were observed in the background susceptibilities (RVP, DSZ and RG) and due to data scatter (e.g., PK) (Table 1; Fig. 2b).

Differences in the background susceptibility of loess have been recognized for the DSZ ($18.6 \times 10^{-8} \text{ m}^3/\text{kg}$) and RVP ($30.3 \times 10^{-8} \text{ m}^3/\text{kg}$) sediments, where significantly higher background susceptibility is observed compared to the average $13.04 \times 10^{-8} \text{ m}^3/\text{kg}$ and median $10.03 \times 10^{-8} \text{ m}^3/\text{kg}$ values. In contrast, significantly lower background susceptibility was found in the RG section ($4.4 \times 10^{-8} \text{ m}^3/\text{kg}$) (Table 1; Fig. 2b, red arrow).

Increased scattering of data appears in samples with low χ_{lf} , for example, PK loess. Sediment samples with χ_{lf} values below $\sim 40 \times 10^{-8} \text{ m}^3/\text{kg}$ exhibit a less significant relation between paedogenic enhancement (scattering χ_{fs}) and bulk magnetic susceptibility (χ_{lf}). This is seen in the scattered data distributions observed for the DSZ and PK sections (Fig. 2c and d). These samples are characterized by 1) relatively high χ_{lf} and low χ_{fs} compared to others (e.g., DSZ; Fig. 2c, dotted line circle) or 2) relatively low χ_{lf} but high χ_{fs} (e.g., PK and a group of samples from TI; Fig. 2d, dashed line circles).

Profile (ref); [n-number of samples]	Loess region	Equation of magnetic enhancement trend	r, [p(a)<0.05]	Backg. susc. ($\times 10^{-8}$ m ³ /kg)
Raigorod (RG; Költringer et al. 2020); [216]	East European Plain	$y = 39.87x + 4.3659$	0.93	4.4
Paks (PK) (4 kHz); [141]	Middle Danube Basin	$y = 26.532x + 10.04$	0.95	10.0
Paks (PK) (16 kHz); [141]	Middle Danube Basin	$y = 44.219x + 10.04$	0.95	10.0
Semlac (Se; Zeeden et al., 2016); [215]	Middle Danube Basin	$y = 15.846x + 10.294$	0.99	10.3
Titel composite section (TI; Marković et al., 2011); [1229]	Middle Danube Basin	$y = 16.391x + 10.383$	0.99	10.4
Srednaya Akhtuba (SA; Költringer et al., 2020); [103]	East European Plain	$y = 19.695x + 12.296$	0.56	12.3
Leninsk (LN; Költringer et al., 2020); [315]	East European Plain	$y = 8.0712x + 14.882$	0.57	14.9
Dunaszekcső (DSZ; Újvári et al., 2016); [315]	Middle Danube Basin	$y = 16.944x + 18.561$	0.99	18.6
Rasova-Valea cu Pietre (RVP; Zeeden et al., 2018); [348]	Lower Danube Basin	$y = 16.67x + 30.333$	0.90	30.3
Stalać (ST; Obreht et al., 2016); [410]	Lower Danube Basin	$y = 25.111x + 93.001$	0.67	93.0

Table 1. Summary of the magnetic enhancement trends in the studied sections of the ELB.

Beyond recent magnetic measurements from Paks, other magnetic susceptibility data are collected from Költringer et al. (2020), Marković et al. (2011), Obreht et al. (2016), Újvári et al. (2016) and Zeeden et al. (2016, 2018).

4.2 Rock magnetic characteristics of PK loess samples

Rock magnetic and SEM analyses were conducted on selected PK samples located in

the region, which display significant scatters in the χ_{lf} vs. χ_{fs} plot (Fig 2, black triangles

and dots).

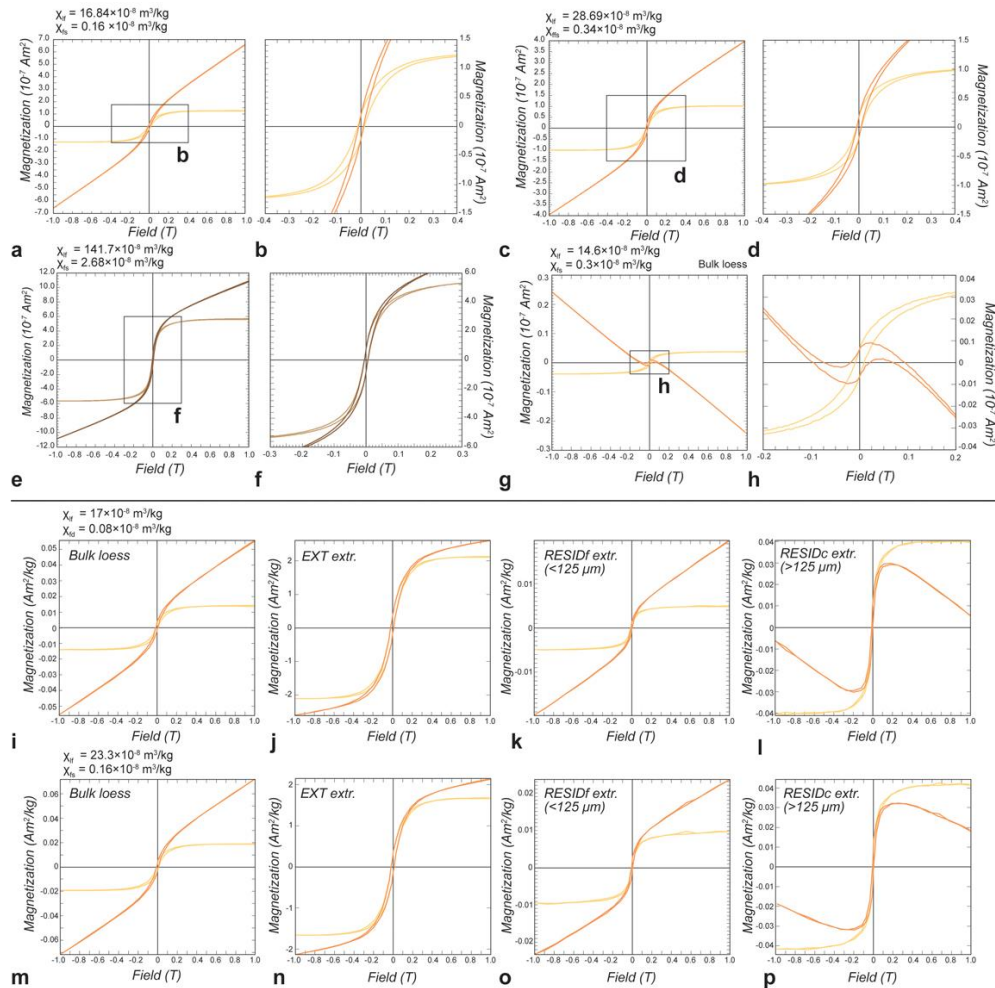


Figure 3. Comparison of hysteresis curves of aeolian, non-weathered loess (a-d), a well-

developed paleosol horizon (e and f), and an aeolian loess unit with low χ_{lf} but relatively

high χ_{fs} (g and h) compared to the normal range χ_{fs} of loess (Fig. 2d; sediment samples

located close to the trendline of the “true loess line” and samples in the lower right area

of the plot, indicated by dashed lines). The orange and dark brown curves indicate the noncorrected values, and the yellow and light brown curves indicate the hysteresis loop after para- and diamagnetic correction. The hysteresis curves starting at panel i) display the results from bulk, EXT and RESID samples; bulk loess samples before extraction (i and m), EXT (j and n), RESIDf (k and o) and RESIDc (l and p).

The hysteresis curves of the selected samples from PK loess, characterized by a low χ_{lf} and variable χ_{fs} (Figs. 3a-d), are very similar to those of the paleosol sample from PK (Figs. 3e and f). An unusual hysteresis loop was identified in one sample from the PK section with a high χ_{fs} and one of the lowest χ_{lf} values; the presence of diamagnetic material with ferrimagnetic contribution is revealed by the appearance of a ferrimagnetic loop in the diamagnetic hysteresis curve (Fig. 3g and h). Similar hysteresis curves were also identified during the study of RESIDc (Fig. 3l and p).

The hysteresis loops of the loess sample closed at higher fields than the paleosol curve (Fig. 3a-f, i, j, m and n). This phenomenon can relate to a higher coercivity (antiferromagnetic) component in loess (Necula and Panaiotu, 2012).

The ratio of coercivity of remanence (remanent coercive force) to coercivity (H_{cr}/H_c) ranges from approximately 2.2 to 4.0 for all samples, with some values of approximately

5. The ratio of saturation remanence to saturation magnetization (M_{rs}/M_s) ranged from approximately 0.11 to 0.17 for all samples, along with irregular values such as ~2 and 2.7 (Fig. 4). Based on the study of Dunlop (2002), such M_{rs}/M_s and H_{cr}/H_c ratios may indicate increasing amount of SD (and SP) contributors in the sediment samples, characterized by low χ_{lf} , but high χ_{fs} (Fig. 1, and 4).

Bulk loess samples and some of the RESIDf samples are in the region defined by H_{cr}/H_c : ~3-3.8 and M_{rs}/M_s : ~0.11 to 0.18 values). This region overlaps with that of loess samples from the CLP (Fukuma and Torii, 1998). Based on the improved Day plot (Dunlop, 2002), the samples fall into the region of the mixture of MD and SD grains (previously defined as PSD), with 15-25% SD content (Fig. 4). EXT and RESIDc samples contain slightly higher relative amounts of SD contributors (ca. 20-30%), based on their H_{cr}/H_c : ~2-2.8 and M_{rs}/M_s : ~0.11 to 0.15 values (Fig. 4).

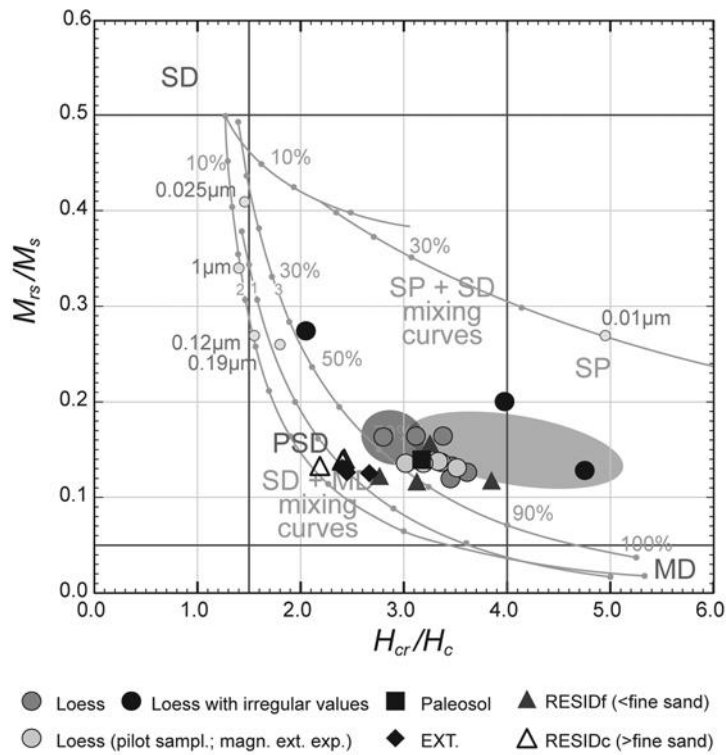


Figure 4. Magnetic domain (grain size) characteristics of the studied PK samples, revealed by Day plot analysis. The location of the samples indicates the characteristic magnetic domain (grain size) of the magnetic contributors. The PSD region indicates grains ~ 0.7 to $15 \mu\text{m}$ in diameter (magnetite; Nagy et al., 2019), the SD region indicates grains $< 0.7 \mu\text{m}$ (Nagy et al. 2019) and $< 15 \mu\text{m}$ (SD haematite; Dunlop, 1981), and the MD region indicates grains $> 15 \mu\text{m}$ in diameter (magnetite; Nagy et al., 2019). The light grey and dark grey areas represent the loess and paleosol samples from Xifeng, Chinese Loess Plateau (Dunlop, 2002).

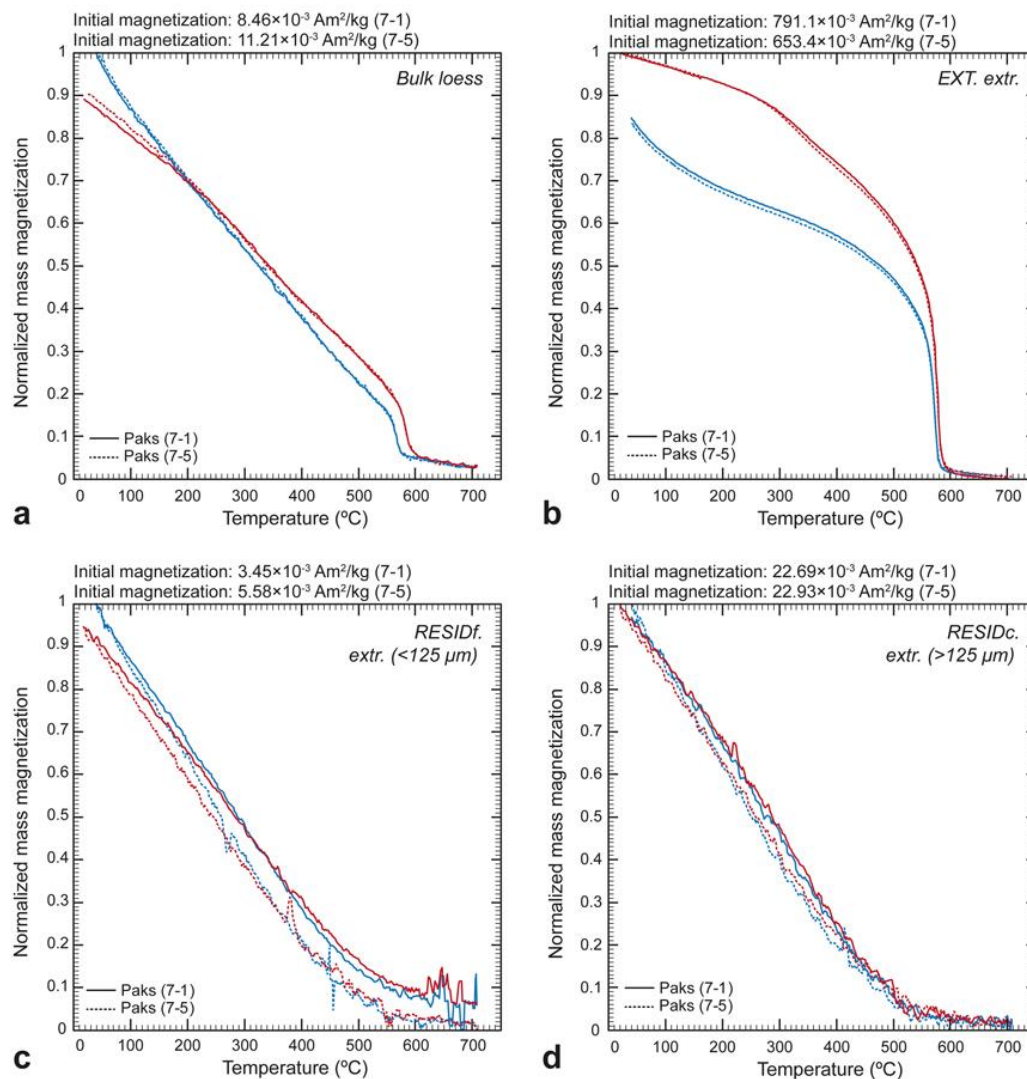


Figure 5. Results of thermomagnetic experiments on bulk loess (a), EXT (b), RESIDf, (c) and RESIDc (d) extracts. The red/blue curves indicate the heating/cooling phases.

Thermomagnetic analysis of bulk pilot samples from PK loess and on EXT and various grain size RESID extracts may allow the decomposition of the thermomagnetic curves of natural loess samples. The magnetization of bulk loess changes gradually until ~580 °C. Above ~580 °C, a drop in magnetization indicates the T_c of magnetite (585 °C).

There is still a weak magnetization above the T_c of magnetite, which may be related to haematite and fades with increasing temperature at approximately 700 °C (Fig. 5a). A hump was observed at ~250-300 °C on the heating curve of the EXT sample. An irreversible cooling curve (started about 560 °C) consists of a section below 200 °C where the cooling curve “crosses” the heating curve, and the initial magnetization is lower than the final magnetization after cooling to room temperature. It may indicate some mineral alteration during the experiment, which may occur above 200 °C. The hump may indicate the conversion of thermally unstable maghemite (Gao et al., 2019). Compared to bulk loess, the most characteristic feature of the heating curve is the drop around the T_c of magnetite (~580 °C) (Fig. 5b). Instead of this feature, which is completely missing in the thermomagnetic curves of RESIDf and c extract, the most characteristic feature is the gradual change of the magnetization (Fig. 5c and d). The gradual decrease in magnetization reaches near zero magnetization at approximately 500-550 °C and may reflect the blocking temperature of finer-grained (SD) (titano)magnetite (e.g., Day, 1975; Dunlop and Özdemir, 1997).

4.3 Binocular and scanning electron microscopy

Due to the possible appearance of very fine-grained magnetic contributors in loess

identified by the magnetic methods above and some observed dark coloured patches on/in muscovite crystals during binocular microscope observation (Fig. 6a-c), SEM imaging was performed on the non-magnetic extracts, especially, but not limited to, muscovite minerals. The elemental map shows the appearance of submicron-level iron oxides along with Pb inclusions in muscovite (Fig. 6d and e).

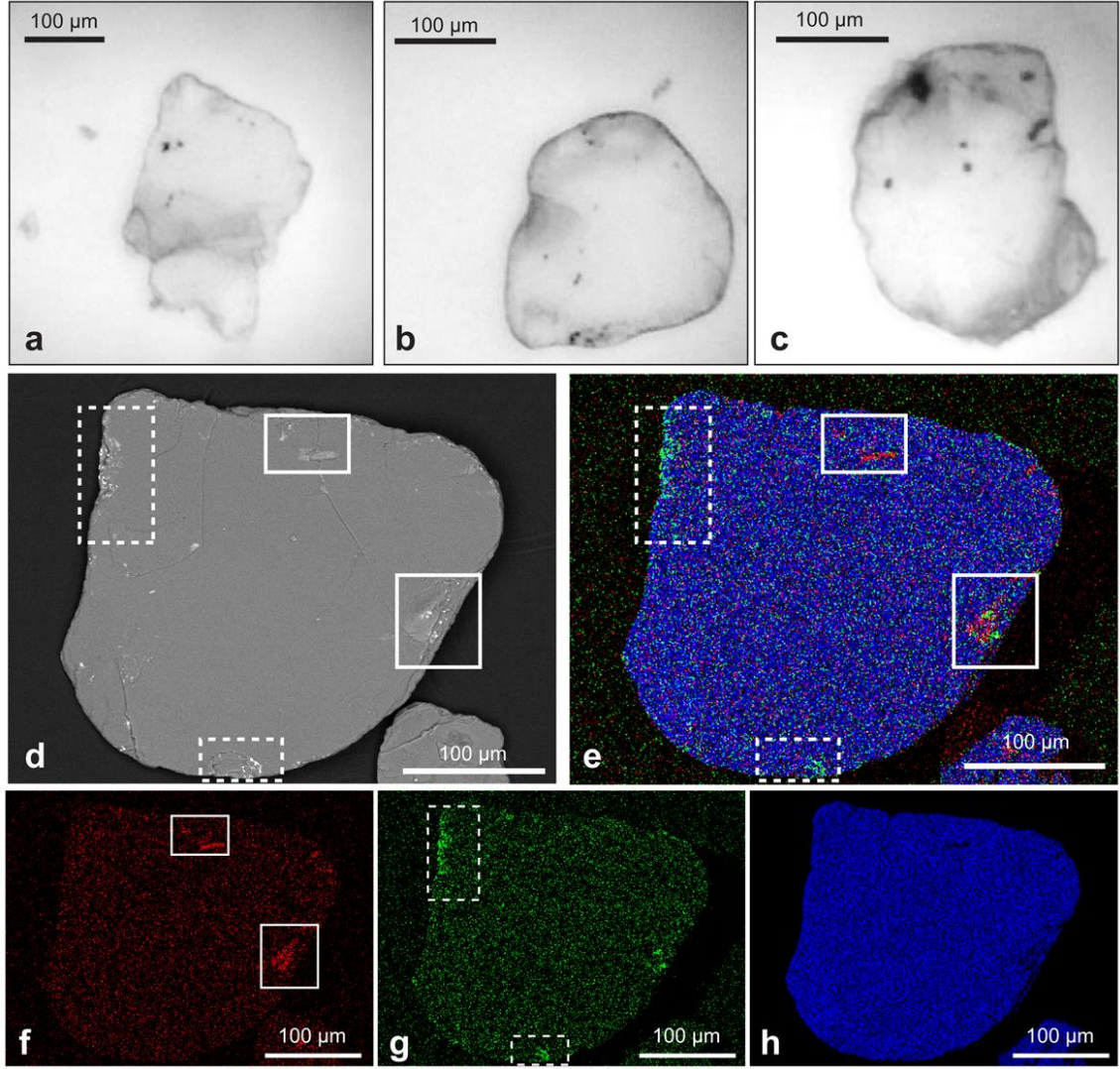


Figure 6. Binocular (a, b, and c) and scanning electron microscopy (d - backscattered electron image and e - elemental scan image) images of muscovite grains from aeolian

loess without any obvious sign of pedogenesis. The reddish areas denoted in solid line boxes indicate higher concentrations of iron. The greenish areas denoted by dashed line boxes indicate higher Pb concentrations, possibly related to galenite (PbS). Figure 6f, g and h are the corresponding element maps of the elemental scan image (Figure 6e), showing the Fe, Pb and Si element maps respectively.

The EDS from the areas of increasing Pb and Fe concentration (Fig. 7a, c and e) and from inclusions (Fig. 7b, d and f) both show a similar, but blended composition: although the components of muscovite(-chlorite) dominate the EDS, Pb and Fe peaks are also recognisable (Fig. 7). The mixed composition and the less characteristic appearance of the Pb and Fe peaks might be caused by the limitation of the instrument, which prevents us to reveal clear EDS of submicron size objects (e.g. the inclusions from Fig. 7b).

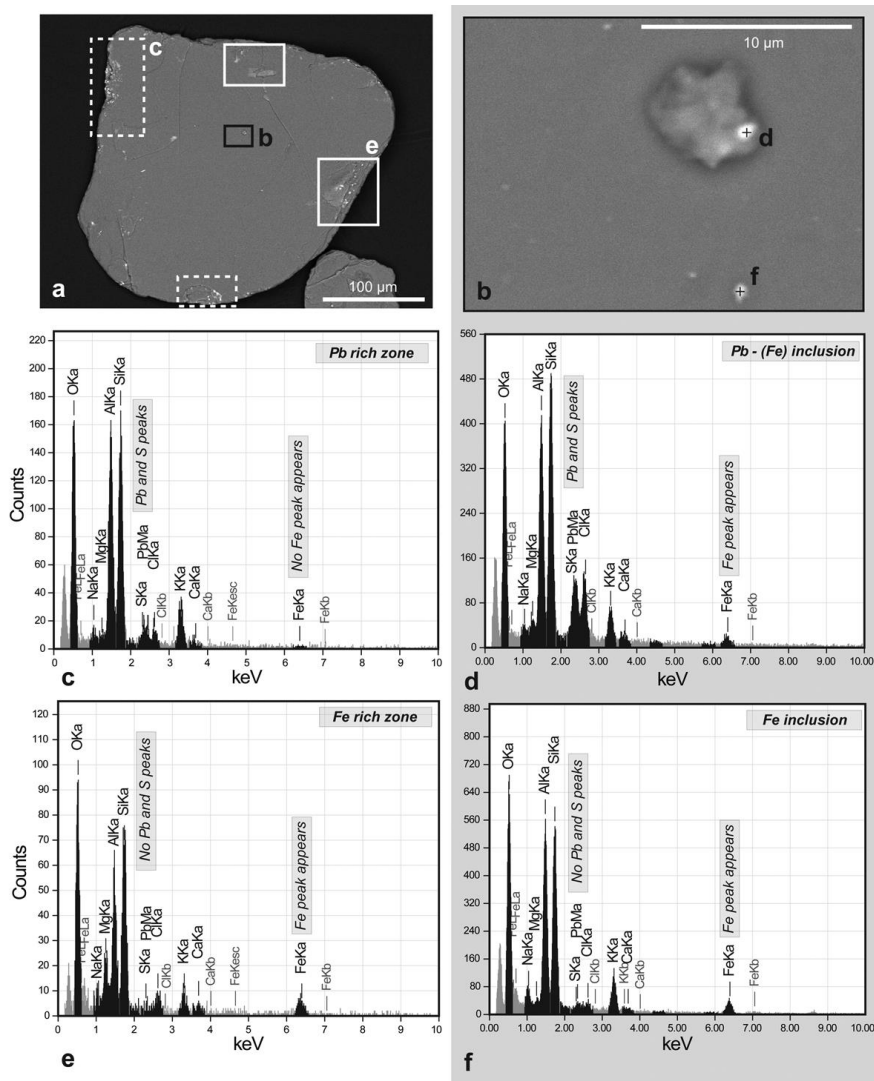


Figure 7. The characterization of the (magnetic) inclusions in muscovite from PK loess.

a) One of the studied muscovite grains with regions characterized by increasing concentration of Pb and Fe (see Fig. 6d-h); b) surface and subsurface micron to submicron size inclusions in the grain; c and e) EDS representing the elemental composition of regions with increasing Pb (c) and Fe (e) content; and d and f) EDS of the inclusions, appearing on Figure 7b. The grey background connects the EDS related to the inclusions, observed in Figure 7b.

565

566 Signs of physical and chemical weathering on grains are also identified in the studied
567 micrographs (Fig. 8) of sediment samples from the PK profile (characterized by low χ_{lf}
568 and relatively high χ_{fs}). Submicron-sized, fragmented grains were found in sandy loess,
569 possibly indicating physical weathering during deposition and diagenesis (Fig. 8a and b).
570 Steps formed by conchoidal fractures (physical weathering) and partially altered by
571 solution/precipitation structures (pits and channels) and coarse grains fully covered by a
572 weathered surface can also be found in the same sediment unit (Fig. 8c and d).

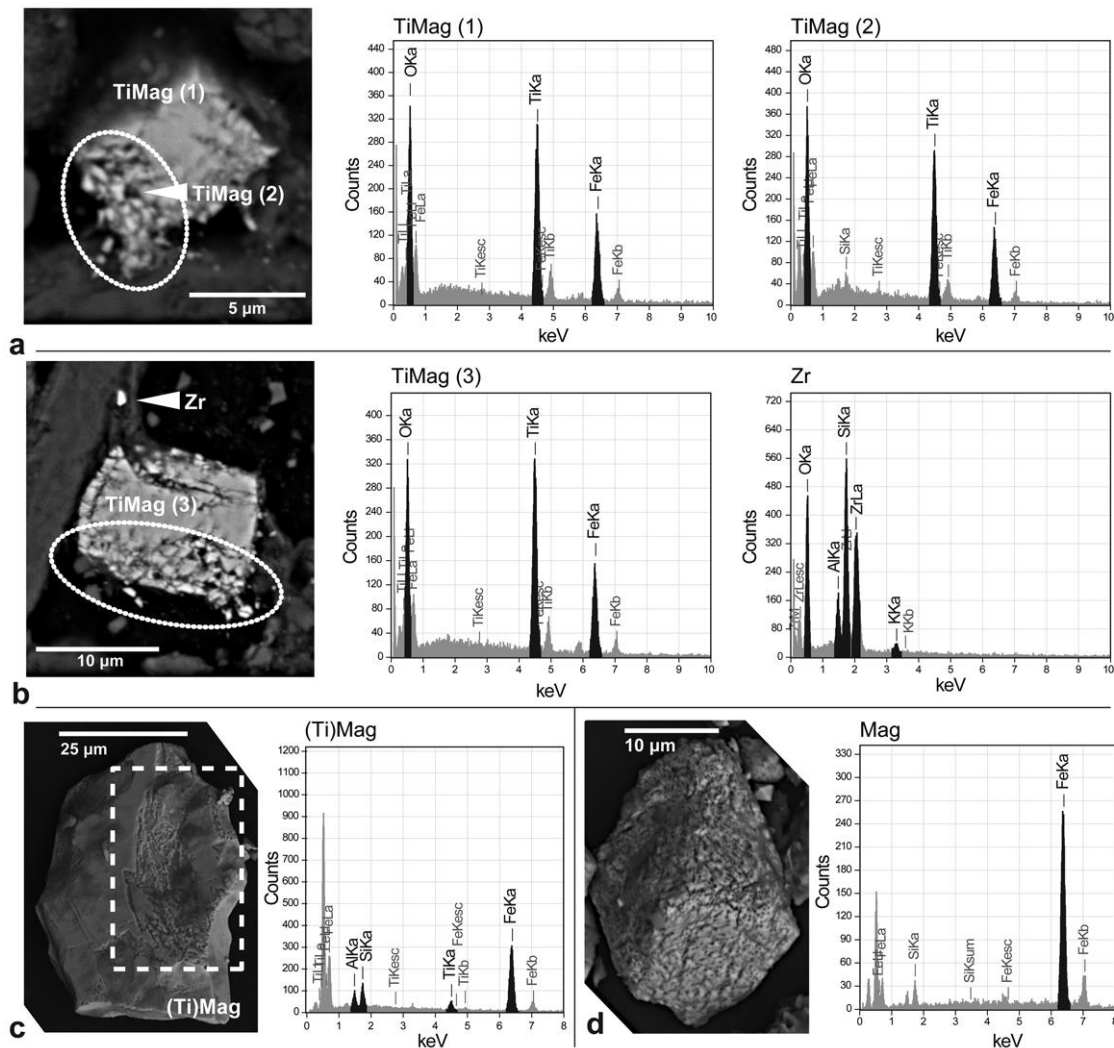


Figure 8. Nanofragmentation of titanomagnetite grains in samples from PK loess, indicated by low χ_{lf} and relatively high χ_{fs} (a and b). The areas marked by dotted line shapes demonstrate the physical weathering of the edge of coarser grains and the detachment of submicron size, fine-grain fragments. The effect of physical and chemical weathering on the grain surface (c). The area indicated by the dashed line box marks conchoidal fracture steps partially altered by solution/precipitation structures (pits and channels; more information about weathering marks in Vos et al., 2014, and Makvandi et

al., 2015). Example of magnetite with identical crystallographic planes but covered by pits (d), the sign of precipitation on the grain surface. Mineral types were identified by energy dispersive spectroscopy: Mag – magnetite, TiMag – titanomagnetite, and Zr – zircon.

5. Discussion

Figure 9. shows a summary of the key mechanisms (discussed in Section 5.1 and 5.2 in detailed) which may influence the enhancement of the magnetic susceptibility parameters during glacial-interglacial cycles. The “cycle of the enhancement of magnetic susceptibility” starts even before the transportation of dust. Differences in the magnetic parameters of the source materials of dust may cause significant differences in the magnetic susceptibility parameters of loess. The differences in the depositional environment (e.g. wind speed and interaction between grains) may influence the concentration and characteristic grain size of magnetic grains (Fig. 9; orange arrows). In contrast of the dry and arid dust depositional periods, chemical weathering may appear even during a slightly milder and humid periods, causing alteration on the surface of the particles. The influence of weathering (physical and chemical alteration, pedogenesis),

biogenic activity (e.g. formation of bacterial magnetite) and/or increasing (vertical) mineral migration and dissolution (e.g. in the body of the paleosol), triggered by the increasing precipitation and warmer temperature, is getting stronger during interglacial periods by during interglacial periods (Fig. 9; red arrows). The cycle of the enhancement of magnetic susceptibility signal restarts with the subsequent glacial period, following the interglacial with cooling, aridification and increasing dust accumulation (Fig. 9; blue arrows). As it is shown in Figure 9 and below in Section 5.1 and 5.2, processes, influencing the magnetic susceptibility parameter values in opposite way may appear parallel, causing complex magnetic enhancement. Therefore, the enhancement of magnetic susceptibility parameters cannot be described by one, exclusive model.

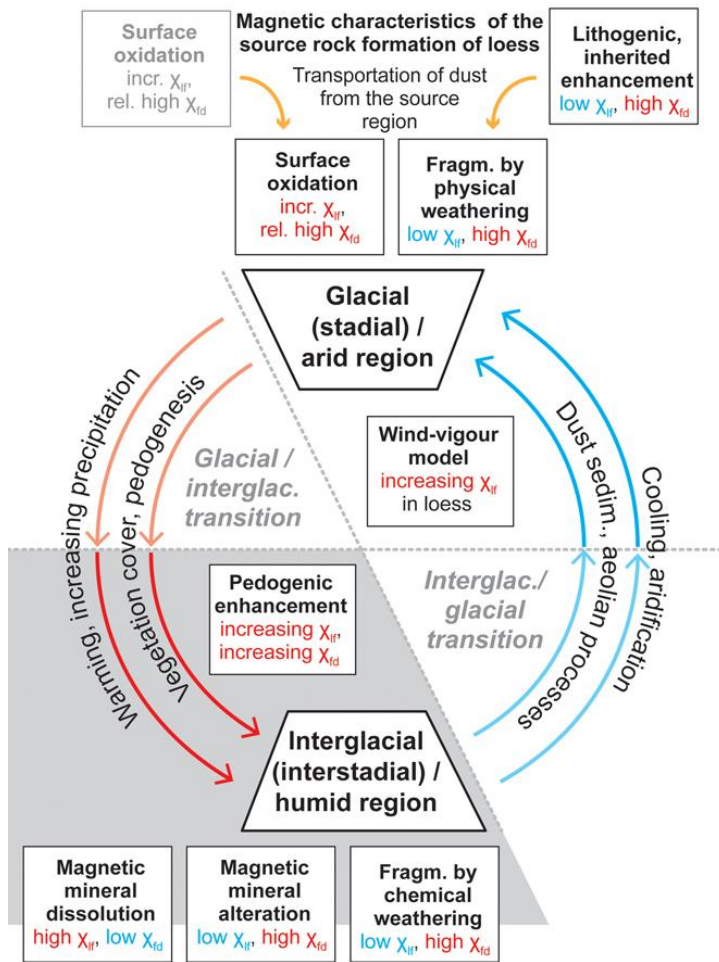


Figure 9. Cycle of the enhancement of magnetic susceptibility in loess and the summary of some key magnetic enhancement mechanisms in loess with an influence on χ_{lf} and $\chi_{fd(fs)}$ parameters during Quaternary glacial and interglacial periods. The grey region is characterized by increasing precipitation, temperature, pedogenic processes (red arrows) and intense chemical weathering. The blue arrows indicate cooling, aridification, increasing aeolian activity and dust accumulation. The yellow arrows mark dust transportation from the source area of loess.

5.1 Complexities in the the magnetic enhancement trend

The results above demonstrate that the pedogenic enhancement model explains the trends seen in most studied loess sequences (Table 2; Fig. 2) (e.g., Maher and Taylor, 1988; Heller et al., 1993; Forster et al., 1994; Dearing et al., 1996; Maher 2011, 2016; Zeeden et al., 2016, 2018). This implies that the amount of authigenic magnetic minerals increases during pedogenesis in the studied sediments (Fig. 2, Fig. 9). The pedogenic enhancement trends, observed, for example, in the SA, SE and TI successions, agree with this model. The trend lines and the allocation of the samples in the χ_{fs} vs χ_{lf} plot of the LN, PK, RG, RVP and DSZ sections point to deviations (Fig. 2b, c and d; Fig. 9). The type of these deviations from the “true loess line” found in the characteristics of the enhancement trends and from the study of the relationship between χ_{fs} and χ_{lf} are summarized below (Table 2; Fig. 9).

Theories, models	Phenomena	Short description	Loess region	References (e.g.)
Pedogenic enhancement model	increasing χ_{lf} , increasing χ_{fd}	Magnetic enhancement of loess by in situ authigenic mineral forming during paedogenesis	CLP, ELB,	Heller et al. (1993); Maher et al. (1994, 2002, 2003); Panaiotu et al. (2001); Orgeira et al. (2011)
Wind-vigour model	low χ_{lf} in paleosols, high χ_{lf} in loess	Increasing input of dense magnetic particles by stronger,	Alaska, Siberia, ELB	Begét and Hawkins (1989); Chachula et al. (1998)

		more frequent winds during glacial periods		
Lithological differences in the source area of the dust (theoretical)	low χ_{lf} in paleosols, high χ_{lf} in loess	Different source area of dust during glacial and interglacial periods	Pampean loess	Schellenberger et al. (2003)
Combined pedogenic and wind-vigour model	low χ_{lf} and high χ_{fd} in paleosols, high χ_{lf} in loess	The combination of the two main theories described above	Central Asia, CLP, ELB, Pampean loess, Siberia	Bidegain et al. (2005); Wang et al. (2006); Kravchinsky et al. (2008); Stevens et al. (2020)
Magnetic mineral dissolution	high χ_{lf} , low χ_{fd}	Dissolution of mainly fine-grain magnetic contributors by hydromorphic processes	ELB	Taylor et al. (2014)
Magnetic mineral alteration	low χ_{lf} , relatively high χ_{fd}	The gradual conversion of magnetite and maghemite to goethite in a humid environment (~940 mm/year)	Australian loess/parna	Ma et al. (2013)
Fragmentation by chemical weathering	low χ_{lf} , relatively high χ_{fd}	Destruction of coarse (detrital sedimentary) magnetic particles by strong weathering in paleosols	ELB	Bidegain et al. (2009); Baumgart et al. (2013); Gocke et al. (2014); Ghafarpour et al. (2016)
Surface oxidation ("detrital magnetic enhancement")	incr. χ_{lf} , relatively high χ_{fd}	Surface oxidation of coarse magnetic grains, and ultrafine magnetic mineral forming on their surface	ELB	Buggle et al. (2014); Wacha et al. (2018); Zeeden et al. (2018); Stevens et al. (2020)
Nanofragmentation (by physical weathering)	low χ_{lf} , relatively high χ_{fd}	Fragmentation of coarser sedimentary magnetic particles by physical processes during transportation and diagenesis	ELB	in this study
Lithogenic inherited magnetic enhancement, "lithogenic enh."	low χ_{lf} , relatively high χ_{fd}	Inherited fine-grain magnetic inclusions in phyllosilicates from the source rock of the dust	ELB	in this study

Table. 2. Summary of various magnetic enhancement models explaining the behaviour of χ_{lf} and $\chi_{fd(fs)}$ parameters in loess and paleosol units.

Based on the theory behind the pedogenic enhancement model, the statistical relationship between χ_{fs} and χ_{lf} is characterized by the r correlation coefficient. The r coefficient represents how strong the relationship is between the formation of fine-grain magnetic contributors (indicated by χ_{fs}) and χ_{lf} . In other words, a high r value may indicate that the enhancement is solely due to the neoformation of fine-grained magnetic contributors (e.g., SE and TI profiles). In contrast, low r values suggest 1) that the χ_{fs} and χ_{lf} values are similar, which means uniform paedogenic enhancement levels among the units of succession; i.e. only one type of material (loess or paleosols, with quasi-uniform magnetic susceptibility parameters) appears in the studied section, or 2) a scattering of the data (see 4.1.2).

In the case of low r , the background susceptibility of the studied sequence, i.e., the parameter representing the susceptibility of non-enhanced sediment, may suggest specific processes having an influence on the χ_{fs} and χ_{lf} parameters. For instance, while ST sediments show a low r ($r = +0.67$, $p(a) < 0.05$, $n = 410$) together with extremely high background susceptibility ($93 \times 10^{-8} \text{ m}^3/\text{kg}$), the background susceptibilities of SA ($r =$

+0.56, $p(a) < 0.05$, $n = 103$; $12.3 \times 10^{-8} \text{ m}^3/\text{kg}$) and LN ($r = +0.57$, $p(a) < 0.05$, $n = 315$; $14.9 \times 10^{-8} \text{ m}^3/\text{kg}$) are close to the average value ($13.04 \times 10^{-8} \text{ m}^3/\text{kg}$) characteristic of most sections (Table 1; Fig. 2). The low correlation coefficient associated with high background susceptibility in ST loess may indicate that the studied material is already strongly influenced by pedogenic processes (high pedogenic susceptibility) or originally the sediment itself has high detrital susceptibility compared with other studied sediments. SA and LN loess are characterized by low correlation coefficients associated with average background susceptibility, which suggests that no strong pedogenic enhancement appeared in the loess/paleosols of these sections.

Differences in the background susceptibility from the one defined by Zeeden et al. (2016)'s "true loess line" can be observed in the RVP, DSZ, and RG profiles (Table 2; Fig. 2b, red arrows). For DSZ ($18.6 \times 10^{-8} \text{ m}^3/\text{kg}$) and RVP ($30.3 \times 10^{-8} \text{ m}^3/\text{kg}$), higher background susceptibilities are observed compared to the average value of $13.04 \times 10^{-8} \text{ m}^3/\text{kg}$. These higher values probably represent detrital enhancement, i.e., the deposited dust originally had higher magnetic fractions. By contrast, significantly lower background susceptibility was found for the RG section ($4.4 \times 10^{-8} \text{ m}^3/\text{kg}$), potentially indicating a very low magnetic mineral content of dust or the depletion of magnetic contributors during sedimentation.

Greater scatter in the data was recognized in samples with low χ_{lf} ($\sim 40 \times 10^{-8}$ m³/kg) from DSZ and PK loess (Fig. 2). The scattering exhibits two characteristic patterns in the χ_{fs} vs. χ_{lf} plot (Fig. 2; Fig. 9): 1) low χ_{fs} but relatively high χ_{lf} (Fig. 2c, area separated by dotted oval) and 2) relatively low χ_{lf} but high χ_{fs} (Fig. 2d, area separated by dashed oval).

The *wind vigour effect* may be indicated by the scattered data of DSZ and RVP showing low $\chi_{fd(fs)}$ and relatively high χ_{lf} in loess (Fig. 2c; Fig. 9). It is likely that these factors reflect the increasing input of dense magnetic particles by stronger, more frequent wind gusts during glacial periods, similar to the cases from Alaska (e.g., Begét and Hawkins, 1989), Siberia (Chachula et al., 1998) and the European Loess Belt (Wacha et al., 2018; Zeeden et al., 2018) (Table 2).

The less known or overlooked theory about relatively high χ_{lf} associated with low χ_{fs} , which appeared in DSZ and RVP loess, may be caused by the *dissolution of fine magnetic minerals* (Table 2). Chemical weathering (dissolution) of magnetic mineral components, preferentially starting with the finest magnetic mineral contributors, may be responsible for the significant decreases in the fine-grain components of loess, causing decreasing $\chi_{fd(fs)}$ values (Taylor et al., 2014). However, this hypothesis may not apply to samples from, e.g., the DSZ sequence, which have not experienced significant weathering reported from the sediment units (Újvári et al., 2016).

687 Among the studied sections, some samples with scattered PK data and a group of
688 samples from TI show significant deviations from their main magnetic enhancement
689 trends towards relatively increased χ_{fs} (Fig. 2, area marked by red dashed oval). There are
690 some hypotheses that may describe such features (see below; Table 2; Fig. 9).

691 Bidegain et al. (2009) observed a lower χ_{lf} associated with an increasing χ_{fd} in
692 Pampean loess (Argentina). They attributed this feature to paedogenesis, which resulted
693 in the *weathering of coarser magnetic grains in the parent material* (i.e., decreases in χ_{lf})
694 but increases in the ultrafine-grained particles. Baumgart et al. (2013) reported high χ_{fd}
695 associated with relatively low χ_{lf} in paleosols and attributed the phenomenon to the effect
696 of strong weathering on detrital magnetic particles. The observed “reversed trend of
697 decreasing χ_{lf} with increasing χ_{fd} was considered as weathering of larger magnetic mineral
698 grains” in Nussloch loess as well (Gocke et al., 2014; p. 307). The destruction of coarser
699 magnetic grains may result in increasing χ_{fs} in the studied PK loess (Fig. 2d, area marked
700 by red dashed oval), but chemical alteration can be ruled out (i.e., there are no signs of
701 strong weathering or paedogenesis).

702 Similar to Baumgart et al. (2013), Ma et al. (2013) reported rather high χ_{fd} and low
703 χ_{lf} from Australian aeolian deposits (Mackenzie’s Waterholes Creek - MWC profile) and
704 described the phenomenon as a result of *magnetic mineral alteration*. During chemical

alteration, magnetite and maghemite gradually converted to more stable goethite in a humid environment (expected ~940 mm/year based on modern annual precipitation data), causing χ_{lf} to decrease (Table 2). In the Middle Danube Basin, approximately 200-350 mm/year annual precipitation is estimated during the sedimentation of loess, and even during the paedogenic periods, it might not have reached 700 mm/year (Panaiotu et al., 2001; Bradák et al., 2011). As such, strong weathering processes as the cause of unusual magnetic susceptibility parameters may be excluded in the case of PK and TI loess.

Buggle et al. (2014), Wacha et al. (2018) and Zeeden et al. (2018) proposed the *formation of ultrafine grains on the surface of coarser magnetic hosts* by surface oxidation of MD magnetic grains as a cause of increasing χ_{fd} in sediments (i.e. “detrital magnetic enhancement”) before the influence of pedogenesis (Table 2; Fig. 9). In the case of PK or TI loess, the likelihood of surface oxidation in coarser grains cannot be excluded or verified as a cause of increasing χ_{fs} from analysis of susceptibility alone; therefore, additional rock magnetic and SEM analyses were performed on samples from PK (see below in 4.2).

Dual processes, *the competing appearance of pedogenic magnetic enhancement and the wind-vigour effect*, may offer an alternative explanation for the low χ_{lf} (wind-vigour effect) and higher $\chi_{fs(fd)}$ (pedogenic enhancement). Such a combination of magnetic

enhancement was observed in loess successions, e.g., in the Tibetan Plateau (Wang et al., 2006) and in Siberian loess (Kravchinsky et al., 2008) (Table 2), but due to the lack of any sign of pedogenesis in the mentioned samples from Paks, the case of “dual enhancement” can be excluded (Fig. 2).

5.2 Additional observations on the potential causes of increasing χ_{fs} in PK loess

5.2.1 Fine-grained magnetic contributors of PK loess

The formation of submicron-sized magnetic particles on the surface of coarser magnetic grains may explain the increasing χ_{fs} in samples with low χ_{lf} from PK loess.

The magnetic domain size of both loess and paleosols from the PK site falls into the PSD or mixed MD and SD region (Dunlop, 2002) (Fig. 4). Similar to what was seen in the selected samples from PK loess (Fig. 4), analyses from Alaska (Lagroix and Banerjee, 2002), the CLP (e.g., Liu et al., 1992; Pan et al., 2002; Jin and Liu, 2010; Li et al., 2018) and ELB (e.g., Taylor et al., 2014; Necula et al., 2015) report that PSD or mixed MD and SD state (with 10-30% SD contribution) components are the main magnetic contributors both to loess and paleosol units.

The study of both bulk loess and separated EXT, RESID_f and c extracts from the same loess samples helps to uncover various ways of magnetic enhancement in sediments.

RESIDc extracts, dominated by coarse grains ($>125\text{ }\mu\text{m}$; fine sand), are characterized by PSD (mixed SD and MD) character and show slightly higher (cc. 20-30%) SD contents than the natural samples (Day plot, Fig. 4). This observation suggests that coarser contributors may somehow be associated with ferrimagnetic grains, including SD grains in the RESIDc extract, which dominantly contain dia- and ferromagnetic minerals. The differences between the saturation magnetization of the non-corrected and corrected hysteresis loops indicate significant amounts of high coercivity/dia- and paramagnetic components in PK pilot samples (Richter and van der Pluijm, 1994) (Fig. 3a-f). A high ratio of paramagnetic contributors may influence the magnetic susceptibility values as well. As suggested by Rochette (1987) and Hrouda and Jelinek (1990), for materials characterized by low magnetic susceptibility ($\kappa_{lfav} < 5 \times 10^{-4}$ SI), the paramagnetic components contribute significantly to the low field magnetic susceptibility value. In PK loess, which consists of larger amounts of paramagnetic contributors compared to the ferrimagnetic components, a low susceptibility value may also suggest significant paramagnetic contributions. In addition to the influence of paramagnetic minerals on χ_{lf} , paramagnetic minerals (e.g., phyllosilicates) may function as a host of nanosized ferromagnetic inclusions as well (see below).

5.2.2 Potential signs of surface weathering, inclusions and “nanofragmentation”

The bulk samples from PK loess exhibit somewhat complex magnetic character, including significant paramagnetic, SD and MD, and mainly low coercivity (magnetically soft) contributors such as magnetite and maghemite (Figs. 3, 4 and 5). Such a complex magnetic character is similar to the general magnetic character of loess, reported from various loess regions (e.g., Maher, 2011, and the references therein). In addition, the following features in the thermomagnetic curves (Fig. 5) and in the SEM micrographs may provide additional information about the magnetic enhancement of PK loess samples (Figs. 5, 6, 7 and 8).

1) Appearance of maghemite as a potential indicator of surface weathering. Along with coarser grained MD magnetite (indicated by its T_c at 585 °C, for example), the magnetic extract contains unstable maghemite, revealed by an inflection point (a bump) on the heating curve at approximately 250 °C, indicating its decomposition (Gao et al., 2019) (Fig. 5b). Maghemite seems to be a common contributor in loess-paleosol sequences, as it has been identified in loess (e.g., Evans and Heller, 1994; Liu et al., 2003; Liu et al., 2010; Bradák et al., 2018a, b) as well as paleosol horizons (e.g., Deng et al., 2000, 2001; Zhu et al., 2001; Gao et al., 2019).

Unstable maghemite forms by chemical alteration, which makes it a sensitive

environmental proxy (Gao et al., 2019). Maghemite appearing in sediments may indicate weak weathering during a slightly warmer/wetter phase within the cold and dry sedimentation period in glacials (Stevens et al., 2020). However, an alternative explanation follows the detrital magnetic enhancement theory, as suggested by Buggle et al. (2014). This study proposes that the formation of fine-grained maghemite (PSD and SD grain size) on the surface of coarser grains occurs before/during the sedimentation of dust. Based on the rock magnetic study of loess, Spassov et al. (2003) suggest the appearance of similar features in Chinese loess, i.e., loess detrital magnetite with a weathered crust of maghemite. Weathering and chemical alteration of the surface of coarser grains was observed on SEM images of PK loess, which may support the view of Buggle et al. (2014) or Gao et al. (2019) (Table 2; Fig. 8c and d).

2) Appearance of ferrimagnetic inclusions in para- and diamagnetic loess components.

Hysteresis and thermomagnetic experiments on RESID_f and c extractions from loess samples from the PK sequence (especially coarse, muscovite dominant grains; >125 µm) reveal key information about the magnetic enhancement of sediments. The weak, gradual decreasing magnetization, which reaches zero below the expected T_c of magnetite, may indicate that SD grains of various sizes gradually reach their unblocking temperature (e.g., Day, 1975; Dunlop and Özdemir, 1997) (Fig. 5c and d). In addition, the hysteresis curve

of those coarse-grained nonferromagnetic samples shows a somewhat complex pattern: a diamagnetic curve with a ferromagnetic loop (Fig. 3l and p). Similar hysteresis loops were also observed in some natural samples with low χ_{lf} and higher χ_{fs} in PK loess (Fig. 3g and h). This type of hysteresis loop is rare for loess; to the best of our knowledge, no similar case has yet been reported from loess profiles. The appearance of this curve suggests that the magnetic properties of the studied loess sample are mainly characterized by diamagnetic contributors, but ferrimagnetic components may appear. The weak influence of the ferromagnetic contributors (and the increasing influence of para- and diamagnetic minerals) is already suggested by the very low χ_{lf} (see above at the end of 4.2.1, and in Rochette, 1987; Hrouda and Jelinek, 1990), but the following experiments were needed to reveal the nature of ferromagnetic components.

The similarities between these hysteresis loops of natural samples and RESIDf and c extracts (Fig. 3g-h, l and p) were explored further by SEM experiments. SEM observations on RESIDc extracts of loess (Fig. 6 and 7) showed diamagnetic hysteresis curves, similar to natural samples (Fig. 3l and p). The SEM analyses also indicate the appearance of submicron-scale ($\leq 0.5\text{-}0.6\text{ }\mu\text{m}$) magnetic components (Figs. 6d, e and 7) in natural sediments as well as in RESIDc extracts. The elemental mapping of individual muscovite grains suggests that such components may appear as inclusions in coarser grain

813 phyllosilicate carriers (Fig. 6d and e; Fig. 7) (Table 2).

814 Such inclusions have already been reported from well-developed paleosols as a result
815 of in situ pedogenic mineral neoformation (Yang et al. 2013; Sano et al. 2017; Hyodo et
816 al. 2020). The observation of ferromagnetic inclusions in muscovite from loess without
817 the sign of pedogenesis supports an alternative mode of origin (Fig. 6 and 7). These
818 identified nanosize components in sediments may be traced back to their primary source
819 rock lithologies, formed during various lithogenic processes as inclusions, e.g., in micas
820 (“lithogenic enhancement”) (e.g., Dunlop et al. 2006). Following the physical weathering
821 of the source rocks, the micas with ferromagnetic inclusions were transported from their
822 provenance (in the case of PK, from the Alps and Carpathians) and from local sources,
823 e.g., alluvial fans (Újvari et al. 2012; Thamó-Bozsó et al. 2014), during glacials and
824 (re)deposited as loess sediments. Iron oxide inclusions observed in muscovite (Fig. 6e
825 and 7) can be regarded as a potential source of “lithogenic enhancement” in the
826 sediment(s) from PK. Along with magnetite, galenite inclusions also appear, which are
827 characteristic components in certain magmatic and metamorphic rocks (e.g., granite). In
828 the region of Paks, there is a potential geological formation that contains a significant
829 amount of galenite. In the so-called Velence Granite Formation (Velence Mts., W.
830 Hungary; Fig. 1), galenite appears as a result of regional high-temperature fluid flow

events of a hydrothermal system of Mid- to Late-Triassic age related to the regional heating of the granite (Benkó et al., 2014). These hydrothermal processes might also be responsible for the formation of iron-oxide inclusions (e.g., Nadoll et al., 2014). Following the weathering and erosion of the Velence Granite Formation, component minerals (e.g., muscovite) of granite containing galenite and magnetite would have been transported and redeposited in the Paks region as constituents of loess. This observation supports the study of Schellenberger et al. (2003), who emphasized the importance of lithological differences in the source area of the dust for magnetic enhancement.

3) Physical weathering and nanofragmentation of coarser grains. As suggested by Bidegain et al. (2009), Baumgart et al. (2013) and Gocke et al. (2014) (Table 2), strong chemical weathering of coarser magnetic contributors may cause relatively low χ_{f} but increasing $\chi_{\text{fd(fs)}}$ in paleosol horizons of loess successions. However, weathering processes may not be limited to paleosol horizons and do not necessarily require conditions conducive to strong chemical weathering to fragment coarser grains, as shown in SEM micrographs (Fig. 8a and b). Based on the SEM observations of PK samples with no marks of strong chemical alteration, there is one more process that may form nanosize magnetic particles in the sediments: fragmentation during deposition (e.g., by the collision of grains) and during diagenesis (e.g., by compaction). The formation of

nanosized fragments increases the χ_{fs} of the sediment, but the χ_{lf} (i.e., the concentration of magnetic contributors) does not change. The appearance of nanofragmentation in loess sediments may indicate increasing physical weathering during transportation associated with strengthening of the transport agent. The strengthening of the wind and/or the forgoing fluvial processes before the aeolian “redeposition” results in the transportation of coarser grains and intensifies grain collision and fragmentation.

The three processes summarized above potentially influence the magnetic enhancement in the case of low χ_{lf} associated with high χ_{fs} in apparently unweathered loess. The mentioned processes may contribute to more robust palaeoenvironmental reconstructions in loess by, e.g., indicating weak weathering processes over short, moderate-to-humid periods during loess sedimentation (maghemitization) and marking “harsher” cold periods with the intensification of winds (nanofragmentation).

6. Conclusions

The two generally accepted models (pedogenic and wind-vigour) used to explain the enhancement of magnetic susceptibility parameters in loess apparently do not cover the

867 full range of potential causes of magnetic enhancement in loess. Uncommon cases are
868 indicated by “suspicious horizons”, characterized by high background susceptibility,
869 lower χ_{lf} but higher χ_{fs} , and vice versa.

870 Despite the popularity of magnetic susceptibility parameters and the growing number
871 of irregular cases observed, knowledge about the causes of magnetic enhancement in
872 loess is still limited. Combined scanning electron microscopy (SEM) and magnetic
873 analyses suggest possible causes of increased χ_{fs} in non-altered sediments: the
874 nanofragmentation of coarser grains and the appearance of significant amounts of fine
875 magnetic inclusions in dia- and paramagnetic components, e.g., in muscovite.

876 Such nanoscale magnetic inclusions may originate from various igneous and
877 metamorphic processes, which developed inclusions in phyllosilicates and appear as
878 mineral components in the dust source rock (“lithogenic enhancement”). Following the
879 physical weathering of the rocks containing the magnetically enhanced micas, the grains
880 would be transported from their provenance to the loess regions and be (re)deposited as
881 aeolian loess during glacial periods. Increasing transport energy may lead to the
882 mobilization of coarser grains, rolling and bombardment of the surface. Crushing of
883 coarser grains may lead to physical weathering and the formation of fine, submicron size
884 components (“nanofragmentation”).

The summary of the methods of magnetic enhancement of loess also showed that pedogenic processes do not always lead to enrichment in magnetic contributors but can cause dissolution and magnetic depletion of certain components. Such processes may be dependent on the type of soils and the characteristics of the environment in which the paleosol formed.

The methods of magnetic enhancement recently discovered in loess may not challenge the significance of the basic models, as suggested earlier, but rather describe an unusual feature observed in loess successions that researchers should consider in their interpretations of magnetic susceptibility data.

Acknowledgements

We are thankful for Professor M. Hyodo (Kobe University, Japan), Á. Carrancho and the Paleomagnetic Laboratory (University of Burgos, Spain) for facilitating the magnetic measurements.

B. Bradák acknowledges the financial support of project BU235P18 (Junta de Castilla y Leon, Spain) and the European Regional Development Fund (ERD), project PID2019-108753GB-C21 / AECI / 10.13039/501100011033 of the Agencia Estatal de Investigación and project PID2019-105796GB-I00 / AECI / 10.13039/501100011033 of

the Agencia Estatal de Investigación. Part of the measurements were conducted during a fellowship awarded to B. Bradák at Kobe University, Japan, by the Japan Society for the Promotion of Science (JSPS; P15328). Part of this study was conducted within the cooperative research programme of the Center for Advanced Marine Core Research, Kochi University (15A001, 16A002, 17A016), with the support of the Japan Agency for Marine-Earth Science and Technology (JAMSTEC). The Swedish Research Council is gratefully acknowledged for funding to TS for part of this project (2017-03888).

We are also thankful for the inspiring ideas and comments of two anonymous reviewers.

References

- Amante, C. Eakins, B.W. 2009. ETOPO1 1 Arc-Minute Global Relief Model: Procedures, Data Sources and Analysis. NOAA Technical Memorandum NESDIS NGDC-24. National Geophysical Data Center, NOAA. doi:10.7289/V5C8276M.
- Batchelor, C.L., Margold, M., Krapp, M., Murton, D.K., Dalton, A.S., Gibbard, P.L., Stokes, C.R., Murton, J.B., Manica, A. 2019. The configuration of Northern Hemisphere ice sheets through the Quaternary. *Nature Communications* (2019) 10:3713, <https://doi.org/10.1038/s41467-019-11601-2>

921 www.nature.com/naturecommunications

922 Bábek, O., Chlachula, J., Grygar, T.M. 2011. Non-magnetic indicators of pedogenesis

923 related to loess magnetic enhancement and depletion: Examples from the Czech

924 Republic and southern Siberia. *Quaternary Science Reviews* 30, 967–979.

925 <https://doi.org/10.1016/j.quascirev.2011.01.009>

926 Balsam, W.L., Ellwood, B.B., Ji, J., Williams, E.R., Long, X., El Hassani, A., 2011.

927 Magnetic susceptibility as a proxy for rainfall: Worldwide data from tropical and

928 temperate climate. *Quat. Sci. Rev.* 30, 2732–2744.

929 doi:10.1016/j.quascirev.2011.06.002

930 Barrón, V., and Torrent, J. 2002. Evidence for a simple pathway to maghemite in Earth

931 and Mars soils. *Geochimica et Cosmochimica Acta* 66, 2801–2806, [https:// doi .org](https://doi.org/10.1016/S0016-7037(02)00876-1)

932 /[10 .1016 /S0016-7037 \(02\)00876 -1](https://doi.org/10.1016/S0016-7037(02)00876-1).

933 Barrón, V., Torrent, J., de Grave, E. 2003. Hydromaghemite, an intermediate in the

934 hydrothermal transformation of 2-line ferrihydrite into hematite. *The American*

935 *Mineralogist* 88, 1679–1688, [https:// doi .org /10 .2138 /am -2003 -11 -1207](https://doi.org/10.2138/am-2003-11-1207).

936 Baumgart, P., Hambach, U., Meszner, S., Faust, D. 2013. An environmental magnetic

937 fingerprint of periglacial loess: Records of Late Pleistocene loess-palaeosol sequences

938 from Eastern Germany. *Quaternary International* 296, 82-93.

939 <https://doi.org/10.1016/j.quaint.2012.12.021>

940 Begét, J.E., Hawkins, D. B. 1989. Influence of orbital parameters on Pleistocene loess
941 deposits in central Alaska. *Nature* 337, 151-153. <https://doi.org/10.1038/337151a0>

942 Benkó, Zs., Molnár, F., Lespinasse, M., Billström, K., Pécskay, Z., Németh, T. 2014.
943 Triassic fluid mobilization and epigenetic lead-zinc sulphide mineralization in the
944 Transdanubian Shear Zone (Pannonian Basin, Hungary). *Geologica Carpathica* 65/3,
945 177-194. DOI: <https://doi.org/10.2478/geoca-2014-0012>

946 Bidegain, J.C., Evans, M.E., van Velzen, A.J. 2005. A magnetoclimatological
947 investigation of Pampean loess, Argentina. *Geophys. J. Int.* 160, 55-62.
948 <https://doi.org/10.1111/j.1365-246X.2004.02431.x>

949 Bidegain, J.C., Rico, Y., Bartel, A., Chaparro, M.A.E., Jurado, s. 2009. Magnetic
950 parameters reflecting pedogenesis in Pleistocene loess deposits of Argentina.
951 *Quaternary International* 209, 175–186. <https://doi.org/10.1016/j.quaint.2009.06.024>

952 Boyle, J., F., Dearing, J., A., Blundell, A., Hannam, J., A. 2010. Testing competing
953 hypotheses for soil magnetic susceptibility using a new chemical kinetic model.
954 *Geology* 38 (12), 1059-1062. <https://doi.org/10.1130/G31514.1>

955 Buggle, B., Hambach, U., Müller, K., Zöller, L., Marković, S. B., Glaser, B. 2014. Iron
956 mineralogical proxies and Quaternary climate change in SE-European loess–paleosol

957 sequences. *Catena* 117, 4–22. <https://doi.org/10.1016/j.catena.2013.06.012>
 958 Bradák, B., Újvári, G., Seto, Y., Hyodo, M., Végh, T. 2018a. A conceptual magnetic fabric
 959 development model for the Paks loess in Hungary. *Aeolian Research* 30, 20–31.
 960 <https://doi.org/10.1016/j.aeolia.2017.11.002>
 961 Bradák, B., Seto, Y., Hyodo, M., Szeberényi, J. 2018b. Relevance of ultrafine grains in
 962 the magnetic fabric of paleosols. *Geoderma* 330, 125–135.
 963 Bradák, B., Seto, Y., Csonka, D., Végh, T., Szeberényi, J. 2019a. The hematite-goethite
 964 enhancement model of loess and an ‘irregular’ case from Paks, Hungary. *Journal of*
 965 *Quaternary Science* 1-10. ISSN 0267-8179. DOI: 10.1002/jqs.3101.
 966 Bradák, B., Seto, Y., Nawrocki, J. 2019b. Significant pedogenic and palaeoenvironmental
 967 changes during the early Middle Pleistocene in Central Europe. *Palaeogeography,*
 968 *Palaeoclimatology, Palaeoecology* 534, 109335.
 969 <https://doi.org/10.1016/j.palaeo.2019.109335>
 970 Cheng, L., Song, Y., Sun, H., Bradák, B., Orozbaev, R., Zong, X., Liu, H. 2019.
 971 Pronounced changes in paleo-wind direction and dust sources during MIS3b recorded
 972 in the Tacheng loess, northwest China. *Quaternary International*.
 973 <https://doi.org/10.1016/j.quaint.2019.05.002> (in press)
 974 Chlachula, J., Evans, M.E., Rutter, N.W. 1998. A magnetic investigation of a Late

975 Quaternary loess/paleosol record in Siberia. *Geophys. J. Int.* 132, 128-132.
976 <https://doi.org/10.1046/j.1365-246x.1998.00399.x>

977 Day, R. 1975. Some curious thermomagnetic curves and their interpretation. *Earth and*
978 *Planetary Science Letters* 27, 95-100. [https://doi.org/10.1016/0012-821X\(75\)90166-1](https://doi.org/10.1016/0012-821X(75)90166-1)

979 Day, R., Fuller, M., and Schmidt V. A. 1977. Hysteresis properties of titanomagnetites:
980 Grain size and composition dependence. *Phys. Earth Planet. Inter.* 13, 260-267.
981 [http://dx.doi.org/10.1016/0031-9201\(77\)90108-X](http://dx.doi.org/10.1016/0031-9201(77)90108-X)

982 Dearing, J. A., Dann, R. J. L., Hay, K., Lees, J. A., Loveland, P. J., Maher, B. A., O'Grady,
983 K., 1996. Frequency-dependent susceptibility measurements of environmental
984 materials, *Geophys. J. Int.*, 124, 228–240. [https://doi.org/10.1111/j.1365-](https://doi.org/10.1111/j.1365-246X.1996.tb06366.x)
985 [246X.1996.tb06366.x](https://doi.org/10.1111/j.1365-246X.1996.tb06366.x)

986 Deng, C., Zhu, R., Verosub, K., Singer, M., Yuan, B. 2000. Paleoclimatic significance of
987 the temperature-dependent susceptibility of Holocene loess along a NW-SE transect
988 in the Chinese Loess Plateau. *Geophysical Research Letters*, 27(22), 3715–3718.
989 <https://doi.org/10.1029/2000GL008462>

990 Deng, C., Zhu, R., Jackson, M., Verosub, K., Singer, M. 2001. Variability of the
991 temperature-dependent susceptibility of the Holocene eolian deposits in the Chinese
992 Loess Plateau: A pedogenesis indicator. *Physics and Chemistry of the Earth, Part A:*

993 Solid Earth and Geodesy, 26(11-12), 873–878. <https://doi.org/10.1016/S1464->
994 1895(01)00135-1

995 Dumas, R.K., Li, C-P., Roshchin, I.V., Schuller, I.K., Liu, K. 2007. Magnetic fingerprints
996 of sub-100 nm Fe dots, Physical Review B 75, 134405.
997 <https://doi.org/10.1103/PhysRevB.75.134405>

998 Dunlop, D. J., 1981. The rock magnetism of fine particles. Phys. Earth Planet. Inter. 26,
999 1-26. [https://doi.org/10.1016/0031-9201\(81\)90093-5](https://doi.org/10.1016/0031-9201(81)90093-5)

1000 Dunlop D. J. 2002. Theory and application of the Day plot (Mrs/Ms versus Hcr/Hc) 2.
1001 Application to data for rocks, sediments, and soils. J. Geophys. Res. 107:No. B3, 2057,
1002 10.1029/2001JB000487, 2002

1003 Dunlop, D. J., Özdemir, Ö., 1997. Rock Magnetism. Fundamentals and Frontiers,
1004 Cambridge Studies in Magnetism Series. Cambridge University Press, Cambridge,
1005 New York, Port Chester, Melbourne, Sydney, 573 p.

1006 Dunlop, D. J., Özdemir, Ö., Rancourt, D. G., 2006. Magnetism of biotite crystals. Earth
1007 and Planetary Science Letters, 243. 805–819.
1008 <https://doi.org/10.1016/j.epsl.2006.01.048>

1009 Evans, M. E., 2001, Magnetoclimatology of aeolian sediments, Geophys. J. Int., 144, 495-
1010 497. <https://doi.org/10.1046/j.0956-540X.2000.01317.x>

1011 Evans, M.E., Heller, F. 1994. Magnetic enhancement and palaeoclimate: study of a
 1012 loess/palaeosol couplet across the Loess Plateau of China. *Geophys. J. Int.* 117, 257-
 1013 264. <https://doi.org/10.1111/j.1365-246X.1994.tb03316.x>
 1014 Forster, T., Evans, M.E. & Heller, F., 1994. The frequency dependence of low field
 1015 susceptibility in loess sediments. *Geophys. J. Int.*, 118, 636–642.
 1016 <https://doi.org/10.1111/j.1365-246X.1994.tb03990.x>
 1017 Fukuma, K., and M. Torii, 1998. Variable shape of magnetic hysteresis loops in the
 1018 Chinese loess-paleosol sequences. *Earth Planets Space* 50, 9-14.
 1019 <https://doi.org/10.1186/BF03352081>
 1020 Gao, X., Hao, Q., Oldfield, F., Bloemendal, J., Deng, C., Wang, L., Song, Y., Ge, J., Wu,
 1021 H., Xu, B., Li, F., Han, L., Fu, Y., Guo, Z. 2019. New high-temperature dependence of
 1022 magnetic susceptibility-based climofunction for quantifying paleoprecipitation from
 1023 Chinese loess. *Geochemistry, Geophysics, Geosystems*, 20, 4273–4291.
 1024 <https://doi.org/10.1029/2019GC008401>
 1025 Geiss, C.E., Zanner, C.W., 2007. Sediment magnetic signature of climate in modern
 1026 loessic soils from the Great Plains. *Quat. Int.* 162–163, 97–110.
 1027 <https://doi.org/10.1016/j.quaint.2006.10.035>
 1028 Geiss, C.E., Egli, R., Zanner, C.W., 2008. Direct estimates of pedogenic magnetite as a

1029 tool to reconstruct past climates from buried soils. *J. Geophys. Res. Solid Earth* 113,
 1030 1–15. <https://doi.org/10.1029/2008JB005669>
 1031 Gocke, M., Hambach, U., Eckmeier, E., Schwark, L., Zöller, L., Fuchs, M., Löscher, M.,
 1032 Wiesenberg, G.L.B., 2014. Introducing an improved multi-proxy approach for
 1033 paleoenvironmental reconstruction of loess–paleosol archives applied on the late
 1034 Pleistocene Nussloch sequence (SW Germany). *Palaeogeogr. Palaeoclimatol.*
 1035 *Palaeoecol.* 410, 300–315. <http://dx.doi.org/10.1016/j.palaeo.2014.06.006>.
 1036 Heller, F., Shen, C.D., Beer, J., Liu, X., M., Liu, T.S., Bronger, A., Suter, M., Bonani, G.,
 1037 1993. Quantitative estimates and palaeoclimatic implications of pedogenic
 1038 ferromagnetic mineral formation in Chinese loess. *Earth Planet. Sci. Letters* 114, 385–
 1039 390. [https://doi.org/10.1016/0012-821X\(93\)90038-B](https://doi.org/10.1016/0012-821X(93)90038-B)
 1040 Hrouda, F., 2011. Models of frequency-dependent susceptibility of rocks and soils
 1041 revisited and broadened, *Geophys. J. Int.*, 187, 1259–1269.
 1042 <https://doi.org/10.1111/j.1365-246X.2011.05227.x>
 1043 Hrouda, F., Jelinek, V., 1990. Resolution of ferromagnetic and paramagnetic anisotropies
 1044 in rock, using combined low-field and high-field measurements. *Geophys. J. Int.* 103,
 1045 75–84. <https://doi.org/10.1111/j.1365-246X.1990.tb01753.x>
 1046 Hu, P., Liu, Q., Torrent, J., Barrón, V., Jin, C. 2013. Characterizing and quantifying iron

1047 oxides in Chinese loess/paleosols: Implications for pedogenesis. *Earth and Planetary*
1048 *Science Letters* 369–370, 271–283. <https://doi.org/10.1016/j.epsl.2013.03.033>

1049 Hu, P., Liu, Q., Heslop, D., Roberts, A.P., Jin, C., 2015. Soil moisture balance and
1050 magnetic enhancement in loess–paleosol sequences from the Tibetan Plateau and
1051 Chinese Loess Plateau. *Earth and Planetary Science Letters* 409, 120–132.
1052 <https://doi.org/10.1016/j.epsl.2014.10.035>

1053 Hyodo, M., Sano, T., Matsumoto, M., Seto, Y., Bradák, B., Suzuki, K., Fukuda, J-i., Shi,
1054 M., Yang, T. 2020. Nanosized authigenic magnetite and hematite particles in mature-
1055 paleosol phyllosilicates: New evidence for a magnetic enhancement mechanism in
1056 loess sequences of China. *Journal of Geophysical Research: Solid Earth*, 125,
1057 e2019JB018705. <https://doi.org/10.1029/2019JB018705>

1058 Ji, J.F., Balsam, W., Chen, J., 2001. Mineralogic and climatic interpretations of the
1059 Luochuan loess section (China) based on diffuse reflectance spectrophotometry.
1060 *Quaternary Research* 56, 23–30. <https://doi.org/10.1006/qres.2001.2238>

1061 Ji, J.F., Balsam, W., Chen, J., Liu, L.W., 2002. Rapid and quantitative measurement of
1062 hematite and goethite in the Chinese loess–paleosol sequence by diffuse reflectance
1063 spectroscopy. *Clays and Clay minerals* 50, 208–216.
1064 <https://doi.org/10.1346/000986002760832801>

1065 Ji, J.F., Chen, J., Balsam, W., Lu, H., Sun, Y., Xu, H., 2004. High resolution hematite/
1066 goethite records from Chinese loess sequences for the last glacial–interglacial cycle:
1067 Rapid climatic response of the East Asian Monsoon to the tropical Pacific.
1068 Geophysical Research Letters 31, L03207. doi:10.1029/2003GL018975.

1069 Jiang, Z., Liu, Q., Colombo, C., Barrón, V., Torrent, J., Hu, P., 2013. Quantification of Al-
1070 goethite from diffuse reflectance spectroscopy and magnetic methods, Geophys. J. Int.
1071 Geomagnetism, rock magnetism and palaeomagnetism, 1-14.
1072 <https://doi.org/10.1093/gji/ggt377>

1073 Jiang, Z., Liu, Q., Roberts, A.P., Barrón, V., Torrent, J., Zhang, Q., 2018. A new model
1074 for transformation of ferrihydrite to hematite in soils and sediments. Geology 46, 1-4.
1075 <https://doi.org/10.1130/G45386.1>.

1076 Jin, C., Liu, Q. 2010. Reliability of the natural remanent magnetization recorded in
1077 Chinese loess. Journal of Geophysical Research 115: B04103,
1078 doi:10.1029/2009JB006703.

1079 Költringer, C.A., Stevens, T., Almqvist, B., Bradák, B., Kurbanov, R., Snowball, I.,
1080 Yarovaya, S. 2020. Mineral magnetic record of Late Quaternary environmental
1081 evolution in Lower Volga loess sequences, Russia. Quaternary Research (under
1082 review), QUA-20-1

1083 Kravchinsky, V.A., Zykina, V.S., Zykin, V.S. 2008. Magnetic indicator of global
1084 paleoclimate cycles in Siberian loess–paleosol sequences. *Earth and Planetary Science*
1085 *Letters* 265, 498-514. <https://doi.org/10.1016/j.epsl.2007.10.031>

1086 Lagroix, F., Banerjee, S. K., 2002. Paleowind direction from the magnetic fabric of loess
1087 profile in central Alaska. *Earth and Planetary Science Letters* 195, 99-102.
1088 [https://doi.org/10.1016/S0012-821X\(01\)00564-7](https://doi.org/10.1016/S0012-821X(01)00564-7)

1089 Leonhardt, R. 2006. Analyzing rock magnetic measurements: The RockMagAnalyzer 1.0
1090 software. *Computers & Geosciences* 32, 1420-1431.
1091 <https://doi.org/10.1016/j.cageo.2006.01.006>

1092 Li, G., Xia, D., Appel, E., Wang, Y., Jia, J., Yang, X. 2018. A paleomagnetic record in
1093 loess–paleosol sequences since late Pleistocene in the arid Central Asia. *Earth, Planets*
1094 *and Space* 70:44. <https://doi.org/10.1186/s40623-018-0814-8>

1095 Liu, Q.S., Barrón, V., Torrent, J., Eeckhout, S., Deng, C. 2008. Magnetism of intermediate
1096 hydromaghemite in the transformation of 2-line ferrihydrite into hematite and its
1097 paleoenvironmental implications: *Journal of Geophysical Research* 113, B01103,
1098 <https://doi.org/10.1029/2007JB005207>.

1099 Liu, Q., Torrent, J., Barrón, V., Duan, Z. Q., Bloemendal, J. 2011. Quantification of
1100 hematite from the visible diffuse reflectance spectrum: effects of aluminium

1101 substitution and grain morphology. *Clay Minerals* 46, 137–147.
 1102 doi:10.1180/claymin.2011.046.1.137
 1103 Liu, X., Shaw, J., Liu, T., Heller, F., Yuan, B. 1992. Magnetic mineralogy of Chinese loess
 1104 and its significance. *Geophys. J. Int.* 108, 301-308. [https://doi.org/10.1111/j.1365-](https://doi.org/10.1111/j.1365-246X.1992.tb00859.x)
 1105 [246X.1992.tb00859.x](https://doi.org/10.1111/j.1365-246X.1992.tb00859.x)
 1106 Liu, X.M., Shaw, J., Jiang, J.Z., Bloemendal, J., Hesse, P., Rolph, T., Mao, X.G., 2010.
 1107 Analysis on variety and characteristics of maghemite, *Sci. China Earth Sci.*, 53, 1–6.
 1108 Liu, Y., Shi, Z., Deng, C., Su, H., Zhang, W. 2012. Mineral magnetic investigation of the
 1109 Taledo loess–palaeosol sequence since the last interglacial in the Yili Basin in the Asian
 1110 interior. *Geophys. J. Int.* 190, 267–277 doi: 10.1111/j.1365-246X.2012.05527.x
 1111 Liu, Z., Liu, Q., Torrent, J., Barrón, V., Hu, P. 2013. Testing the magnetic proxy
 1112 χ_{FD}/HIRM for quantifying paleoprecipitation in modern soil profiles from Shaanxi
 1113 Province, China, *Glob. Planet. Change*, 110, 368–378.
 1114 <https://doi.org/10.1016/j.gloplacha.2013.04.013>
 1115 Long, X., Ji, J., Barr, V., 2016. Climatic thresholds for pedogenic iron oxides under
 1116 aerobic conditions : Processes and their significance in paleoclimate reconstruction.
 1117 *Quat. Sci. Rev.* 150, 264–277. <https://doi.org/10.1016/j.quascirev.2016.08.031>
 1118 Ma, M., Liu, X., Hesse, P.P., Lü, B., Guo, X., Chen, J. 2013. Magnetic properties of loess

1119 deposits in Australia and their environmental significance. *Quaternary International*
1120 296, 198-205. <https://doi.org/10.1016/j.quaint.2012.06.018>

1121 Maher, B. A. 2011. The magnetic properties of Quaternary aeolian dusts and sediments,
1122 and their palaeoclimatic significance. *Aeolian Research* 3, 87–144.
1123 <https://doi.org/10.1016/j.aeolia.2011.01.005>

1124 Maher, B. A. 2016. Palaeoclimatic records of the loess/palaeosol sequences of the
1125 Chinese Loess Plateau. *Quaternary Science Reviews* 154, 23-84.
1126 <https://doi.org/10.1016/j.quascirev.2016.08.004>

1127 Maher, B.A., Taylor, R.M., 1988. Formation of ultrafine-grained magnetite in soils,
1128 *Nature*, 336, 368–370. <https://doi.org/10.1038/336368a0>

1129 Maher, B.A., Alekseev, A., Alekseeva, T., 2002. Variation of soil magnetism across the
1130 Russian steppe: Its significance for use of soil magnetism as a palaeorainfall proxy.
1131 *Quat. Sci. Rev.* 21, 1571–1576. [https://doi.org/10.1016/S0277-3791\(02\)00022-7](https://doi.org/10.1016/S0277-3791(02)00022-7)

1132 Maher, B.A., Alekseev, A., Alekseeva, T., 2003. Magnetic mineralogy of soils across the
1133 Russian Steppe: Climatic dependence of pedogenic magnetite formation. *Palaeogeogr.*
1134 *Palaeoclimatol. Palaeoecol.* 201, 321–341. [https://doi.org/10.1016/S0031-](https://doi.org/10.1016/S0031-0182(03)00618-7)
1135 [0182\(03\)00618-7](https://doi.org/10.1016/S0031-0182(03)00618-7)

1136 Maher, B.A., Thompson, R., Zhou, L.P., 1994. Spatial and temporal reconstructions of

1137 changes in the Asian palaeomonsoon: A new mineral magnetic approach. *Earth Planet.*
 1138 *Sci. Lett.* 125, 461–471. [https://doi.org/10.1016/0012-821X\(94\)90232-1](https://doi.org/10.1016/0012-821X(94)90232-1)
 1139 Makvandi, S., Beaudoi, G., McClenaghan, B.M., Layton-Matthews, D. 2015. The surface
 1140 texture and morphology of magnetite from the Izok Lake volcanogenic massive sulfide
 1141 deposit and local glacial sediments, Nunavut, Canada: Application to mineral
 1142 exploration. *Journal of Geochemical Exploration* 150, 84–103
 1143 Marković S. B., Hambach, U., Stevens T., Kukla, G.J., Heller, F., McCoy, W.D., Oches,
 1144 E.A., Buggle, B., Zöller, L. 2011. The last million years recorded at the Stari
 1145 Slankamen (Northern Serbia) loess-palaeosol sequence: revised chronostratigraphy
 1146 and long-term environmental trends. *Quaternary Science Reviews* 30, 1142–1154.
 1147 <https://doi.org/10.1016/j.quascirev.2011.02.004>
 1148 Marković SB, Stevens T, Kukla GJ, Hambach U, Fitzsimmons KE, Gibbard P, Buggle B,
 1149 Zech M, Guo Z, Hao Q, Wu H, O'Hara Dhand K, Smalley I, Újvári G, Sümegi P,
 1150 Timar-Gabor A, Veres D, Sirocko F, Vasiljević DA, Jary Z, Svensson A, Jović V,
 1151 Lehmkuhl F, Kovács J, Svirčev Z. 2015. Danube loess stratigraphy — Towards a pan-
 1152 European loess stratigraphic model. *Earth-Science Reviews* 148, 228-258.
 1153 <https://doi.org/10.1016/j.earscirev.2015.06.005>
 1154 Mush, D.R. 2007. Loess deposit, origins and properties. In: Elias, S.A. (ed.) *Encyclopedia*

1155 of Quaternary Science, ELSEVIER, pp. 1405-1418.

1156 Nadoll, P., Angerer, T., Mauk, J.L., French, D., Walshe, J. 2014. The chemistry of
 1157 hydrothermal magnetite: A review. Ore Geology Reviews 61, 1-32.
 1158 <https://doi.org/10.1016/j.oregeorev.2013.12.013>

1159 Necula, C., Dimofte, D., Panaiotu, C. 2015. Rock magnetism of a loess-palaeosol
 1160 sequence from the western Black Sea shore (Romania). Geophys. J. Int. 202, 1733–
 1161 1748 doi: 10.1093/gji/ggv250

1162 Obreht, I., Zeeden, C., Hambach, U., Veres, D., Marković, S.B., Böskén, J., Svirčev, Z.,
 1163 Bačević, N., Gavrilov, M.B., Lehmkuhl, F., 2016. Tracing the influence of
 1164 Mediterranean climate on Southeast Europe during the past 350,000 years. Scientific
 1165 Reports 6, 36334.DOI:10.1038/srep36334

1166 Orgeira, M.J., Egli, R., Compagnucci, R.H., 2011. A quantitative model of magnetic
 1167 enhancement in loessic soils, in: Petrovský, E., Ivers, D., Harinarayana, T., Herrero-
 1168 Bervera, E. (Eds.), The Earth's Magnetic Interior. IAGA Special Sopron Book Series
 1169 book series (IAGA, volume 1), pp. 361-397. [https://doi.org/10.1007/978-94-007-](https://doi.org/10.1007/978-94-007-0323-0)
 1170 [0323-0](https://doi.org/10.1007/978-94-007-0323-0)

1171 Pan, Y., Zhu, R., Liu, Q., Guo, B., Yue, L., Wu, H. 2002. Geomagnetic episodes of the
 1172 last 1.2 Myr recorded in Chinese loess. Geophysical Research Letters 29, 1282,

doi:10.1029/2001GL014024

Panaiotu, C.G., Panaiotu, E.C., Grama, A., Necula, C., 2001. Paleoclimatic record from a loess-paleosol profile in Southeastern Romania. *Phys. Chem. Earth, Part A Solid Earth Geod.* 26, 893–898. [https://doi.org/10.1016/S1464-1895\(01\)00138-7](https://doi.org/10.1016/S1464-1895(01)00138-7)

Pye, K. 1987. Aeolian dust and dust deposits. Academic Press, San Diego, CA, 330p.

Richter, C., van der Pluijm, B. A. 1994. Separation of paramagnetic and ferrimagnetic susceptibilities using low temperature magnetic susceptibilities and comparison with high field methods. *Physics of the Earth and Planetary Interiors* 82, 113-123. [https://doi.org/10.1016/0031-9201\(94\)90084-1](https://doi.org/10.1016/0031-9201(94)90084-1)

Roberts, A.P., Pike, C.R., Verosub K.L. 2000. First-order reversal curve diagrams: A new tool for characterizing the magnetic properties of natural samples. *J. Geophys. Res.* 105:28,461-28,465.

Rochette, P., 1987. Magnetic susceptibility of the rock matrix related to the magnetic fabric studies. *J. Struct. Geol.* 9, 1015–1020. [https://doi.org/10.1016/0191-8141\(87\)90009-5](https://doi.org/10.1016/0191-8141(87)90009-5)

Roberts, A. P., Almeida, T. P., Church, N. S., Harrison, R. J., Heslop, D., Li, Y., Li, J., Muxworthy, A. R., Williams, W., Zhao, X. 2017. Resolving the origin of pseudo-single domain magnetic behaviour. *Journal of Geophysical Research: Solid Earth* 122:9534–

1191 9558. <https://doi.org/10.1002/2017JB014860>
 1192 Sano, T., Hyodo, M., Matsumoto, M. & Seto, Y., 2017. Exploration of pedogenic
 1193 nanoscale particles causing magnetic enhancement in Chinese loess deposits, SEM20-
 1194 13, Japan Geoscience Union, JpGU-AGU Joint Meeting 20th – 25th of May, Makuhari
 1195 Messe, Chiba, Japan, 2017. <https://confit.atlas.jp/guide/event->
 1196 [img/jpguagu2017/SEM20-13/public/pdf?type=in](https://confit.atlas.jp/guide/event-img/jpguagu2017/SEM20-13/public/pdf?type=in)
 1197 Schaetzl, R. J., Bettis, E. A., Crouvi, O., Fitzsimmons, K. E., Grimley, D. A., Hambach,
 1198 U., Lehmkuhl, F., Marković, S. B., Mason, J. A., Owczarek, P., Roberts, H. M., (a12),
 1199 Rousseau, D-D., Stevens, T., Vandenberghe, J., Zárata, M., Veres, D., Yang, S., Zech,
 1200 M., Conroy, J. L., Dave, A. K., Faust, D., Hao, Q., Obreht, I., Prud'homme, C., Smalley,
 1201 I., Tripaldi, A., Zeeden, C., Zech, R. 2018. Approaches and challenges to the study of
 1202 loess—Introduction to the LoessFest Special Issue, Quaternary Research 89 (3), 563-
 1203 618. <https://doi.org/10.1017/qua.2018.15>
 1204 Schellenberger, A., Heller, F., Veit, H. 2003. Magnetostratigraphy and magnetic
 1205 susceptibility of the Las Carreras loess–paleosol sequence in Valle de Tafi, Tucumán,
 1206 NW-Argentina. Quaternary International 106–107, 159–167.
 1207 [https://doi.org/10.1016/S1040-6182\(02\)00170-2](https://doi.org/10.1016/S1040-6182(02)00170-2)
 1208 Spassov, S., Heller, F., Kretschmar, R., Evans, M.E., Yue, L.P., Nourgaliev, D.K. 2003.

1209 Detrital and pedogenic magnetic mineral phases in the loess/palaeosol sequence at
 1210 Lingtai (Central Chinese Loess Plateau). *Physics of the Earth and Planetary Interiors*
 1211 140, 255–275. <https://doi.org/10.1016/j.pepi.2003.09.003>
 1212 Stevens, T., Sechi, D., Bradák, B., Orbe, R., Cossu, G., Tziavaras, C., Baykal, Y.,
 1213 Andreucci, S., Pascucci, V. 2020. Abrupt last glacial dust fall over Southeast England
 1214 associated with dynamics of the British-Irish Ice Sheet. *Quaternary Science Reviews*
 1215 250, 106641, <https://doi.org/10.1016/j.quascirev.2020.106641>
 1216 Taylor, S.N., Lagroix, F., Rousseau, D.-D., Antoine, P., 2014. Mineral magnetic
 1217 characterization of the Upper Pleniglacial Nussloch loess sequence (Germany): an
 1218 insight into local environmental processes. *Geophys. J. Int.* 199:1463–1480. doi:
 1219 10.1093/gji/ggu331
 1220 Torrent J, Liu Q, Bloemendal J, Barrón V. 2007. Magnetic Enhancement and Iron Oxides
 1221 in the Upper Luochuan Loess–Paleosol Sequence, Chinese Loess Plateau. *Soil Sci.*
 1222 *Soc. Am. J.* 71 : 1570–1578 doi:10.2136/sssaj2006.0328
 1223 Toucanne, S., Zaragosi, S., Bourillet, J. F., Gibbard, P.L. Eynaud, F., Giraudeau, J., Turon,
 1224 J. L., Cremer, M., Cortijo, E., Martinez, P., and Rossignol, L., 2009, A 1.2 Ma record
 1225 of glaciation and fluvial discharge from the West European Atlantic margin:
 1226 *Quaternary Science Reviews* 28, 2974-2981.

1227 Újvári, G., Varga, A., Ramos, F. C., Kovács, J., Németh, T., Stevens, T., 2012. Evaluating
1228 the use of clay mineralogy, Sr–Nd isotopes and zircon U–Pb ages in tracking dust
1229 provenance: An example from loess of the Carpathian Basin. *Chemical Geology*, 304–
1230 305, 83–96. <https://doi.org/10.1016/j.chemgeo.2012.02.007>

1231 Újvári G, Varga A, Raucsik B, Kovács J. 2014. The Paks loess-paleosol sequence: a
1232 record of chemical weathering and provenance for the last 800 ka in the mid-
1233 Carpathian Basin. *Quaternary International* 319, 22-37.
1234 <https://doi.org/10.1016/j.quaint.2012.04.004>

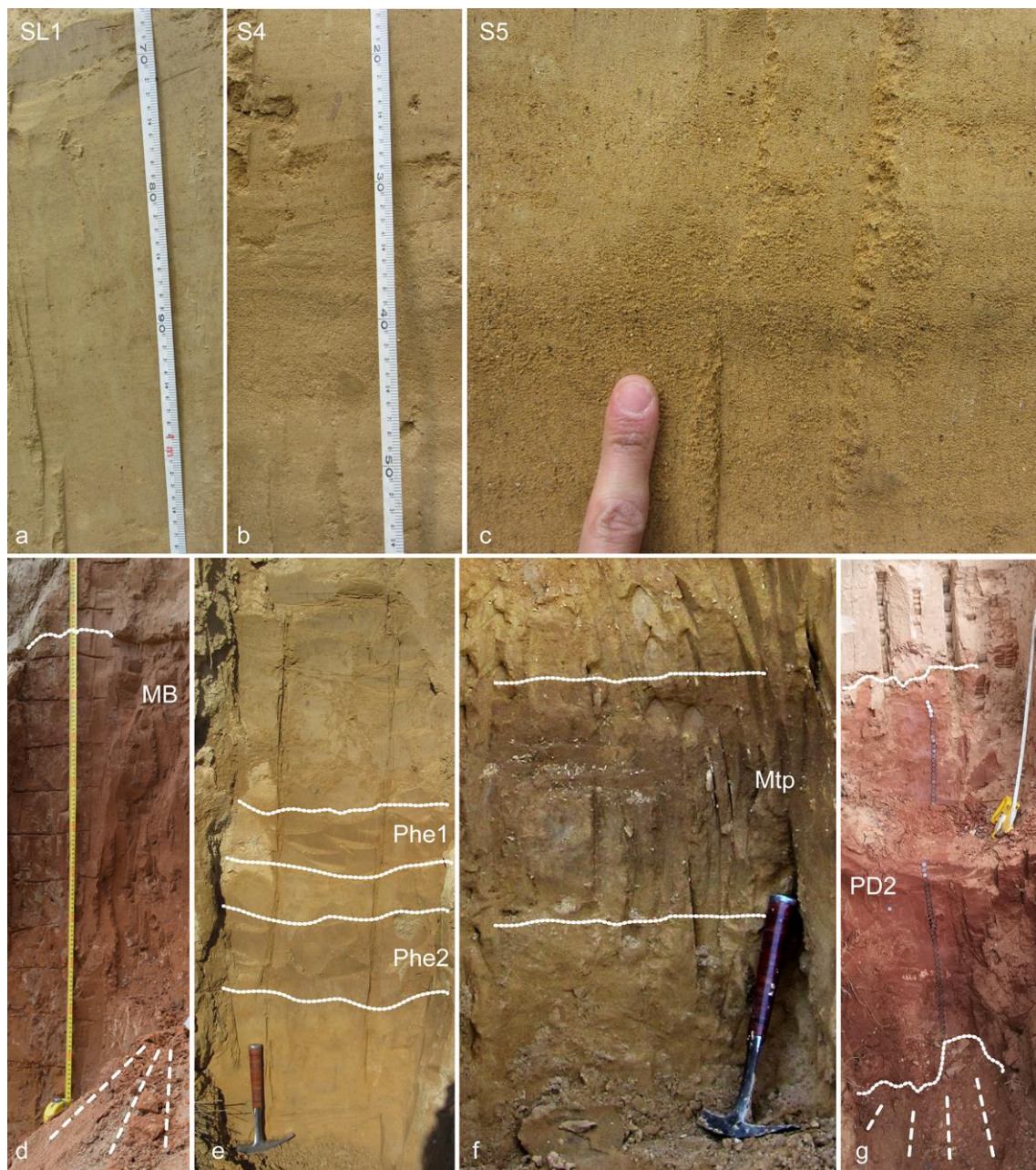
1235 Újvári, G., Kok, J.F., Varga, G., Kovács, J., 2016. The physics of wind-blown loess:
1236 implications for grain size proxy interpretations in Quaternary paleoclimate studies.
1237 *Earth-Science Reviews* 154, 247–278.

1238 Thamó-Bozsó, E., Kovács, L. Ó., Magyari, Á. & Marsi I., 2014. Tracing the origin of
1239 loess in Hungary with the help of heavy mineral composition data, *Quaternary*
1240 *International*, 319, 11–21. <https://doi.org/10.1016/j.quaint.2013.04.030>

1241 Yang, T., Hyodo, M., Zhang, S., Maeda, Yang, Z., Wu, H. & Li, H., 2013. New insights
1242 into magnetic enhancement mechanism in Chinese paleosols, *Palaeogeography,*
1243 *Palaeoclimatology,* *Palaeoecology*, 369, 493–500.
1244 <https://doi.org/10.1016/j.palaeo.2012.11.016>

1245 van Velzen, A.J., Dekkers, M.J., 1999. Low-temperature oxidation of magnetite in loess-
 1246 paleosol sequences: a correction of rock magnetic parameters. *Studia geophysica et*
 1247 *geodaetica* 43 (4), 357-375. <https://doi.org/10.1023/A:1023278901491>
 1248 Vos, K., Vandenberghe, N., Elsen, J. 2014. Surface textural analysis of quartz grains by
 1249 scanning electron microscopy (SEM): From sample preparation to environmental
 1250 interpretation. *Earth-Science Reviews* 128, 93–104.
 1251 <https://doi.org/10.1016/j.earscirev.2013.10.013>
 1252 Wacha, L., Rolf, C., Hambach, U., Frechen, M., Galović, L., Duchoslav, M. 2018. The
 1253 Last Glacial aeolian record of the Island of Susak (Croatia) as seen from a high-
 1254 resolution grain-size and rock magnetic analysis. *Quaternary International* 494, 211-
 1255 224. <https://doi.org/10.1016/j.quaint.2017.08.016>
 1256 Wang, X., Lu, H., Xu, H., Deng, C., Chen, T., Wang, Xi. 2006. Magnetic properties of
 1257 loess deposits on the northeastern Qinghai-Tibetan Plateau: palaeoclimatic
 1258 implications for the Late Pleistocene. *Geophys. J. Int.* 167, 1138-1147, doi:
 1259 10.1111/j.1365-246X.2006.03007.x
 1260 Zeeden, C., Kels, H., Hambach, U., Schulte, P., Protze, J., Eckmeier, E., Marković, S.B.,
 1261 Klasen, N., Lehmkuhl, F. 2016. Three climatic cycles recorded in a loess-palaeosol
 1262 sequence at Semlac (Romania) – Implications for dust accumulation in south-eastern

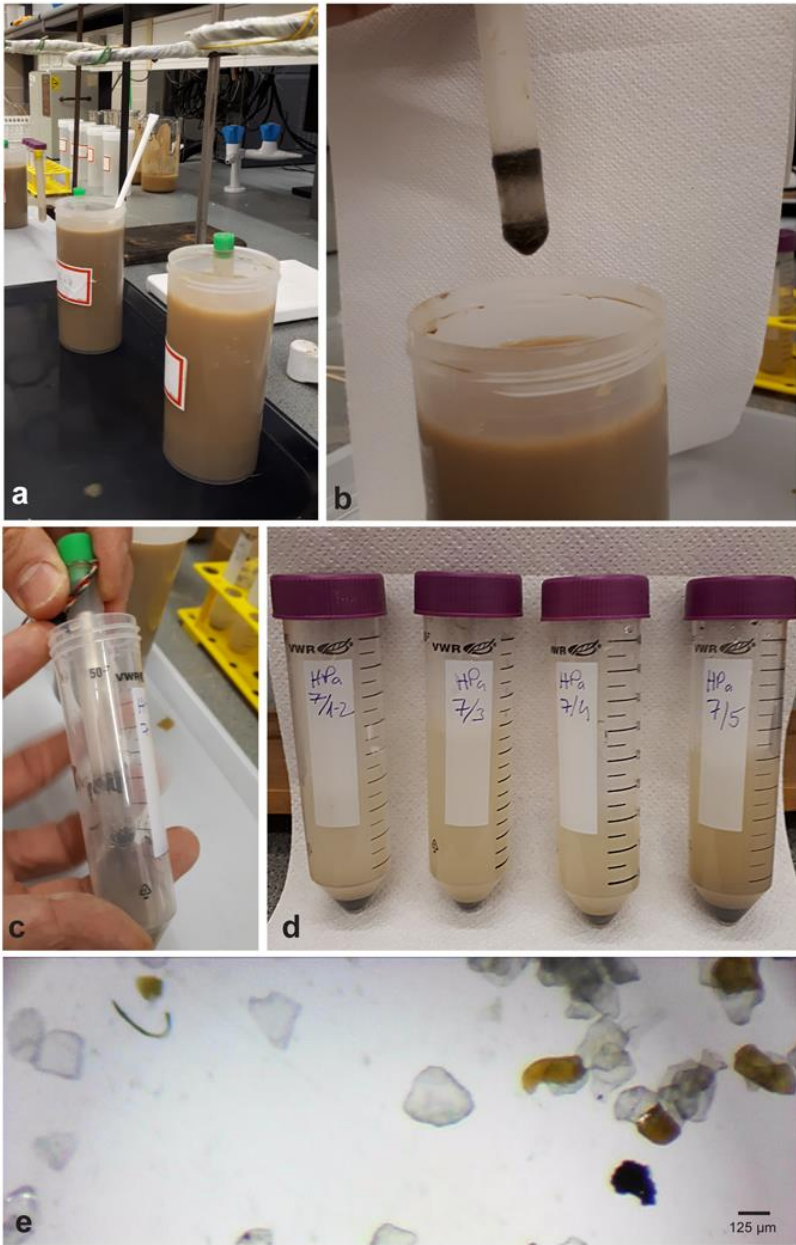
1263 Europe. Quaternary Science Reviews 154, 130-142.
1264 <https://doi.org/10.1016/j.quascirev.2016.11.002>
1265 Zeeden, C., Hambach, U., Veres, D., Fitzsimmons, K., Obreht, I., Böskén, J., Lehmkuhl,
1266 F. 2018. Millennial scale climate oscillations recorded in the Lower Danube loess over
1267 the last glacial period. Palaeogeography, Palaeoclimatology, Palaeoecology 509, 164-
1268 181. <https://doi.org/10.1016/j.palaeo.2016.12.029>
1269 Zhou, L.P., Oldfield, F., Wintle, A.G., Robinson, S.G., Wang, T.J. 1990. Partly pedogenic
1270 origin of magnetic variations in Chinese loess. Nature 346, 737-739.
1271 <https://doi.org/10.1038/346737a0>
1272 Zhu, R., Deng, C., Jackson, M. J. 2001. A magnetic investigation along a NW-SE transect
1273 of the Chinese Loess Plateau and its implications. Physics and Chemistry of the Earth,
1274 Part A: Solid Earth and Geodesy, 26(11-12), 867–872. <https://doi.org/10.1016/S1464->
1275 1895(01)00134-X
1276
1277 Supplementary Materials



Suppl. Mat. 1. Characteristic units of the studied PK section. a) typical aeolian loess from the SL1 sandy loess unit; b and c) fine sand and silt horizons in the S4-S5 units; d) MB (MIS11) paleosol horizon; e) Phe1 and 2 weakly developed paleosol horizons; f) Mtp paleosol unit (MIS15); and g) PD2 (MIS19) paleosol unit. The dashed lines indicate debris.

Separation of EXT, RESIDf and c extractions from loess

- 1. Disintegration of aggregates in ultrasonic bath.
- 2. Separation of fine grain (clay) component from the coarser fraction (silt and above) by laboratory centrifugal separator.
- 3. Separation of EXT extract from suspension by a strong magnet.
- 4. Separation of RESIDf and c by sieve.



1288 **Suppl. Mat. 3.** Collection of various loess magnetic data used in the study.

1289 **Suppl. Mat. 4.** The summary of applied methods, their purpose, the results and their
1290 relation in loess research. a) The setting of strong magnets immersed in the silt-sand
1291 suspensions; b) the EXT extract on the surface of the plastic tube after 24 hours of rest in
1292 the suspension; c) collection of EXT from the surface of the plastic tube; d) EXT, prepared
1293 for drying; and e) phyllosilicates in RESIDc.

1294